J Mol Model (2012) 18:4843–4863
DOI 10.1007/s00894-012-1479-z

ORIGINAL PAPER

Application of docking-based comparative intermolecular contacts analysis to validate Hsp90α docking studies and subsequent in silico screening for inhibitors

Mahmoud A. Al-Sha'er · Mutasem O. Taha

Received: 22 February 2012 / Accepted: 21 May 2012 / Published online: 16 June 2012
© Springer-Verlag 2012

Abstract Heat shock protein (Hsp90α) has been recently implicated in cancer, prompting several attempts to discover and optimize new Hsp90α inhibitors. Towards this end, we docked 83 diverse Hsp90α inhibitors into the ATP-binding site of this chaperone using several docking–scoring settings. Subsequently, we applied our newly developed computational tool—docking-based comparative intramolecular contacts analysis (dbCICA)—to assess the different docking conditions and select the best settings. dbCICA is based on the number and quality of contacts between docked ligands and amino acid residues within the binding pocket. It assesses a particular docking configuration based on its ability to align a set of ligands within a corresponding binding pocket in such a way that potent ligands come into contact with binding site spots distinct from those approached by low-affinity ligands, and vice versa. The optimal dbCICA models were translated into valid pharmacophore models that were used as 3D search queries to mine the National Cancer Institute's structural database for new inhibitors of Hsp90α that could potentially be used as anticancer agents. The process culminated in 15 micromolar Hsp90α ATPase inhibitors.

Keywords Docking · LigandFit · dbCICA · Heat shock protein 90α · Anticancer

Electronic supplementary material The online version of this article (doi:10.1007/s00894-012-1479-z) contains supplementary material, which is available to authorized users.

M. A. Al-Sha'er
Faculty of Pharmacy, Zarqa University,
Zarqa, Jordan
e-mail: a.mahmoud@zu.edu.jo

M. O. Taha (✉)
Drug Discovery Unit, Department of Pharmaceutical Sciences,
Faculty of Pharmacy, University of Jordan,
Amman, Jordan
e-mail: mutasem@ju.edu.jo

Introduction

Heat shock protein 90 (Hsp90) belongs to a family of molecular chaperones that play a pivotal role in the conformational maturation, stability, and functions of protein substrates within the cell. The ATPase activity of Hsp90α provides the energy needed to refold denatured cellular proteins [1]. Amongst the client proteins of Hsp90α are many oncogenes that are essential for the survival, proliferation, invasion, metastasis, and angiogenesis of tumors [2]. In fact, several oncogenic proteins have been shown to be dependent upon Hsp90α for conformational activation, including telomerase, Her2 (erbB2), Raf-1, focal adhesion kinase, and steroid hormone receptors [3].

The validity of Hsp90α as an anticancer target for drug discovery [4, 5] was further established by emerging clinical and preclinical trials employing the potent Hsp90α inhibitor 17-allylamino-17-desmethoxygeldanamycin as well as the natural Hsp90α inhibitors geldanamycin [6], radicicol [7], and other small molecules [8].

The significance of heat shock protein (Hsp90) as a target in anticancer research [1–5, 9–14], combined with the availability of appropriate crystallographic structures for this target [15, 16], prompted us to apply our newly developed computational technique—docking-based intermolecular contacts analysis (dbCICA) [17]—to this target, aiming at the discovery of new Hsp90α inhibitors.

Molecular docking, which is basically a conformational sampling procedure in which various docked conformations are explored to identify the right one, can be a very challenging problem given the degree of conformational

flexibility at the ligand-macromolecular level [18–20]. Docking programs employ diverse methodologies to evaluate different ligand conformations within binding pockets, [21–30], but they must be guided by scoring functions when evaluating the fit between the protein and the corresponding docked ligand(s) [31–37]. The final docked conformations are also selected according to their scores. The accuracy of the scoring function has a major impact on the quality of molecular docking results [22–24, 27, 33, 34, 38–51]. In fact, although modern docking methods are able to calculate the position and orientation of a potential ligand in a receptor binding site fairly accurately, the major problem with them is the inability of scoring functions to evaluate binding free energies correctly, so that different potential ligand–receptor complexes can be ranked [38, 52–56]. The underlying ligand–receptor molecular interactions are highly complex, and various terms should be considered when quantifying the free energy of the interaction process [38, 54, 55, 57–60].

Accordingly, the molecular modeler must find the optimal combination of docking/scoring algorithms capable of correctly ranking docked conformers/poses of potential ligands within a certain binding pocket. Moreover, the molecular modeler must decide whether or not to leave crystallographically explicit water molecules in the binding site prior to ligand docking [61–66]. Furthermore, the fact that crystallographic structures lack information on hydrogen atoms means that it is important to discern, prior to docking, whether or not the ligand's ionizable moieties embedded within the binding site exist in their ionized forms [65, 67]. In this respect, pK_a values can be misleading, since ligand ionizability depends on the local microenvironment within the binding pocket [67].

These problems necessitate the adoption of some measures to validate docking experiments for subsequent structure-based discovery or design [68].

Current validation methods include the following:

(i) Self-docking [69]. However, this technique ignores the fact that docking experiments are usually performed to dock ligands into binding pockets patterned (imprinted) by other co-crystalized ligand(s) (i.e., cross-docking [69]).
(ii) Testing the ability of particular docking configuration to classify compounds in structural databases into actives and inactives [70]. The results are usually presented using receiver operating characteristic (ROC) curves. However, this approach assumes that decoy molecules are inactive, despite a lack of supporting evidence for this [71].
(iii) Validation using 3D-QSAR methods. In this case, a particular docking configuration is considered valid if it succeeds in aligning a set of known ligands (i.e., into the binding pocket) in a 3D alignment capable of explaining bioactivity variations (e.g., via CoMFA) [58, 72, 73]. However, this approach is quite time-consuming and laborious, as CoMFA grids include thousands of energy field points that require energy calculations and then statistical filtering to search for field points that can explain bioactivity variations.

To minimize the drawbacks of molecular docking, and to avoid the inadequacies of existing validation methods, we envisaged dbCICA. This innovative technique assesses any particular docking configuration based on its ability to align a set of ligands (i.e., within a corresponding binding pocket) in such a way that potent ligands come into contact with binding-site atoms distinct from those approached by low-affinity ligands, and vice versa. dbCICA evaluates the consistency of docking by assessing the correlation between ligand affinities and their contacts with binding-site spots. We evaluated the ability of this technique to validate docking configurations against fungal N-myristoyl transferase and glycogen phosphorylase [17].

In the research presented in this paper, we docked 83 Hsp90α inhibitors into the ATPase-binding pocket of this chaperone using LigandFit [29, 74] using different docking conditions and settings. Subsequently, we implemented dbCICA modeling as a tool to measure the success of each set of docking parameters. Thereafter, optimal dbCICA models were employed as templates to generate pharmacophore models that were employed as search queries to screen the National Cancer Institute (NCI) structural database for new GP and CaNMT inhibitors. Hits were subsequently bioassayed. Several hits illustrated good biological properties. We then evaluated the ability of dbCICA to identify the optimal docking conditions. Furthermore, the resulting dbCICA models were used to formulate pharmacophore models that were used as 3D search queries to retrieve new hits from the structural database of the National Cancer Institute (NCI). These hits were subsequently bioassayed. Several hits illustrated low micromolar anti-Hsp90α properties.

Experimental

Molecular modeling

Software and hardware

The following software packages were utilized in the present research:

- CS ChemDraw Ultra, v.11.0 (CambridgeSoft Corp., Cambridge, MA, USA)
- MarvinView, v.5.1.4 (ChemAxon, Budapest, Hungary)
- Discovery Studio (DS) 2.5 (Accelrys Inc., San Diego, CA, USA)

- Ligandfit in Cerius2, v.4.10 (Accelrys Inc.)
- MATLAB, v.R2007a (The MathWorks Inc., Natick, MA, USA)
- Catalyst, v.5.11 (Accelrys Inc.)

Data set

Hsp90

The structures of 83 Hsp90α inhibitors were collected from the literature [75–77]. They were carefully collected to ensure that they had all been bioassayed under similar conditions to allow consistent structure–activity correlation. The in vitro bioactivities of the collected inhibitors were expressed as the concentration of the test compound that inhibited the activity of Hsp90α enzyme by 50 % (i.e., IC_{50}). Figure A and Table A in the "Electronic supplementary material" (ESM) show the structures and IC_{50} values of the collected inhibitors. The logarithms of the measured IC_{50} (μM) values were used in structure–activity correlation, thus yielding a linear correlation between the IC_{50} data and the free-energy changes.

Preparation of ligands

The two-dimensional structures of the collected inhibitors (**1**–**83** in Fig. A and Table A of the ESM) were sketched in ChemDraw Ultra (v.11.0). Two protonation states were assumed for each inhibitor: ionized and unionized, as guided by MarvinView. In the ionized forms, amino substituents ($pK_a \approx 9.0$–9.5) were protonated and given formal positive charges at the appropriate atoms, while carboxylic acids were deprotonated and given formal negative charges at the appropriate atoms. The structures were subsequently converted into reasonable three-dimensional representations using the rule-based conformational methods implemented in DS 2.5, and were saved in the SD format for subsequent docking experiments.

Preparation of crystal structures

The 3D coordinates of Hsp90α were retrieved from the Protein Data Bank (Hsp90α PDB code: 1YET, resolution: 1.9 Å). Hydrogen atoms were added to the protein, utilizing DS 2.5 templates for protein residues. Gasteiger–Marsili charges were assigned to the protein atoms, as implemented within DS 2.5 [78].

The protein structures were utilized in subsequent docking experiments without energy minimization. Explicit water molecules were either retained or removed according to the required docking conditions (i.e., docking in the presence or absence of explicit water molecules).

Docking settings

LigandFit considers the flexibility of the ligand and considers the receptor to be rigid. See the section "SM-3" in the ESM for more details about the LigandFit algorithm [49, 51, 74, 79].

In the current docking experiments, the binding site was generated from the co-crystallized ligand (geldanamycin, GMD), and all 83 ligands in their ionized and unionized forms were docked into the binding site in the presence and absence of explicit water molecules, employing the following docking configurations:

- Monte Carlo search parameters were: number of trials= 15000; search step for torsions with polar hydrogens=30.0°.
- The RMS threshold for ligand-to-binding-site shape matching was set to 2.0 Å, employing a maximum of 1.0 binding-site partitions.
- The interaction energies were assessed employing the CFF force field (v.1.02) with a nonbonded cutoff distance of 10.0 Å and distance-dependent dielectric. An energy grid extending 3.0 Å from the binding site was implemented. The interaction energy was estimated with a trilinear interpolation value using soft potential energy approximations [74].
- Rigid body ligand minimization parameters: 20 steepest descent iterations followed by 40 BFGS-minimization iterations were applied to every orientation of the docked ligand. The best ten poses were further energy-minimized within the binding site for a maximum of 200 rigid body iterations.

High-ranking docked conformers/poses were scored using six scoring functions: Jain [41], LigScore1, LigScore2 [34, 74], PLP1 [79], PLP2 [45], and PMF [49, 51]. Considering each scoring function in turn, the highest-scoring docked conformer/pose of each inhibitor was selected for subsequent 3D-QSAR modeling. This resulted in six sets of 83 docked molecules with scores corresponding to each scoring function. However, the docking and scoring cycle was repeated four times (2 × 2) to cover the different combinations of docking conditions: hydated or nonhydrated binding sites, and ionized or unionized ligands. LigScore1 and LigScore2 scores were calculated employing the CFF force field (v.1.02) and using grid-based energies with a grid extension of 5.0 Å across the binding site. PMF scores were calculated employing cutoff distances of 12.0 Å for carbon–carbon interactions and other atomic interactions.

Docking-based comparative molecular contacts analysis (dbCICA)

The methodology of dbCICA can be described as a series of steps:

(i) The highest-ranking docked pose/conformer of each ligand for a particular docking condition is evaluated to identify its closest atomic neighbors in the binding pocket. Intermolecular atomic neighbors that are closer than (or equal to) a certain predefined distance threshold are assigned an intermolecular contact value of 1; otherwise they are assigned a contact value of 0 (zero). For example, if atom A in the docked ligand is positioned close to atom B in the binding pocket at a distance shorter that the predefined threshold, then this contact is assigned a value of 1. Distance assessment is performed automatically, employing the intermolecular monitor implemented in Discovery Studio v.2.5 [80] combined with a MATLAB script we wrote. Eventually, this step yields a two-dimensional matrix with row labels corresponding to docked ligands (i.e., according to the particular docking–scoring configuration) and column labels corresponding to different binding-site atoms. The matrix is filled with binary code, whereby zeros correspond to interatomic distances above the predefined threshold and ones to distances below (or equal to) the predefined threshold. In the Hsp90α study, three distance thresholds were implemented: 3.5, 2.5, or 2.0 Å. Therefore, three (Hsp90α) binary matrices (corresponding to each distance threshold) were constructed for each docking configuration (i.e., combination of docking engine, scoring function, ligand ionization state, and binding-site hydration status).

(ii) Each individual column in the matrix is regressed against the corresponding molecular bioactivities [i.e., $\log(1/IC_{50})$]. Columns that exhibit a negative correlation with bioactivity are inverted (i.e., zeros are converted to ones and vice versa), and excluded from the subsequent step.

After excluding inverted columns (negative contacts or exclusion volumes), the resulting binary matrix (which is composed of positively correlated contact columns with bioactivity) is then subjected to a genetic algorithm (GA)-based search for the optimal summation of the contact columns that is capable of explaining the variation in bioactivity. In this step, the GA relies on the evolutionary operations of crossover and mutation to select the optimal combination of columns which have summation values that are collinear with the bioactivity variation across the training compounds (see the discussion of GA parameters below). The best column-summation model (single model) is selected as the representative dbCICA model.

The GA can be instructed to output the best dbCICA models resulting from any predefined number of ligand–receptor intermolecular positive contacts, such as the best dbCICA models resulting from sets of two or three or four or five (and so on) concomitant contacts (i.e., summed contact columns). In the current work, we instructed GA to search for the best dbCICA models resulting from two contacts, and to repeat the scan to identify the best summation models for three, four, five, six, seven, eight, nine, and ten contacts. Each set of summed contacts is treated independently to identify the corresponding dbCICA model in each case.

(iii) When using the dbCICA algorithm, there is an option to allow any particular positive contacts column to emerge up to three times in the optimal summation model (i.e., it allows variable weights for contacts). This is performed by implementing dual-valued genes in the GA, where every gene encodes for both the corresponding contact column number and its weight. Column weights are initially randomly distributed in the first generation, and are subsequently subjected to mutation only (not crossover) in GA. This option was allowed in the current work in order to identify intermolecular contacts of higher weights or contributions in the optimal dbCICA models.

(iv) After identifying the optimal summation model(s) based on positive contacts (proportional to bioactivity), dbCICA gets the GA to search for the optimal summation model resulting from combining inverted columns [negatively proportional to bioactivity, see step (ii)] with the optimal positive summation model (s). The user has the option of choosing any number of negative contacts (excluded volumes or steric clashes) to emerge in the final dbCICA model. In the current experiment, we implemented two exclusion settings: either five or ten negative contacts were allowed.

Implementation of the genetic algorithm during dbCICA modeling

The GA toolbox within MATLAB (v.R2007a) was adapted by implementing the following four basic components: the creation function, the crossover function, the mutation function, and the fitness function.

The creation function randomly generates a population of chromosomes of a predefined size (number of summed contact columns, as mentioned in step (ii) in the section "Docking-based comparative molecular contacts analysis (dbCICA)" under "Experimental") in which every chromosome encodes for a certain possible column summation model. Chromosomes differ from one another in the set of summed columns and their weights that they represent.

Crossover children are the offspring created by selecting vector entries (i.e., genes) from a pair of individual chromosomes in the first generation and combining them to form two complementary children, while mutated children are those created by applying random changes to corresponding parents

(i.e., each single parent chromosome is mutated to give a single child by randomly replacing a selected gene in the parent chromosome with another from the chromosome population).

Each chromosome is associated with a fitness value that reflects how good the summation of its encoded genes is compared to those of other chromosomes. The fitness function used in dbCICA can be the correlation coefficient (r^2), the leave-one-out r^2, or the K-fold r^2.

In the current experiments we implemented the fivefold r^2 as the fitness criterion. In this procedure, each chromosome is ranked as follows. The training set is divided into two subsets: the fit and test subsets. The test subset is randomly selected to represent ca. 20 % of the training compounds. This procedure is repeated over five cycles; accordingly, five test subsets with their complementary fit subsets are selected for each chromosome (i.e., column summation model). The five test subsets should cover ca. 100 % of the training compounds as the same compound cannot be selected in more than one test subset. The fit sets are then utilized to generate five submodels employing the same chromosome. The resulting submodels are then utilized to predict the bioactivities of the corresponding testing subsets. Finally, the predicted values of all five test subsets are correlated with their experimental counterparts to determine the corresponding fivefold r^2.

The following parameters were chosen for GA genetic manipulation in the dbCICA of Hsp90α experiments: size of chromosome population=200; rate of mating (crossover fraction)=80 %; elite count=1; maximum number of generations needed to exit from the GA iterations (completing the algorithm)=2000.

Based on these settings, the numbers of each type of child in the offspring generation were as follows: There is one elite child (corresponding to the individual in the parents' generation with the best fitness value), and there are 199 individual children other than the elite child. The algorithm rounds 0.8 (crossover fraction) × 199=159.2 to 159 to get the number of crossover children, and the remaining 40 (i.e., 199–159) are the mutated population. The elite child is passed to the offspring population without alteration.

Molecular field analysis

To validate the dbCICA models, we used comparative molecular field analysis (CoMFA) to assess the ability of corresponding docking-based molecular alignments to yield self-consistent 3D-QSAR models [58, 72, 73]. We used the molecular field analysis (MFA) and the genetic partial least squares (G/PLS) modules implemented in Cerius2® to perform 3D QSAR analysis [58, 72, 73]. See the section "SM-4" in the ESM for experimental details.

Generation of pharmacophores corresponding to successful dbCICA models

In order to utilize dbCICA modeling for effective drug discovery, optimal dbCICA models were used to guide the development of pharmacophoric models to be used as search queries for the discovery of new Hsp90α inhibitors. The pharmacophores were developed through the following steps (see Figs. 2, 3, 4, and 5):

1. Docking configurations that yielded the best dbCICA models were selected (see Tables 1 and 2). The corresponding docked poses/conformers of the most potent compounds (Hsp90α inhibitors of $IC_{50}<$ 0.05 μM) were retained in the binding pocket, while other less potent compounds were discarded.
2. Subsequently, the optimal dbCICA models (i.e., models I, II, or III; Tables 1 and 2) were used to predict the bioactivities of potent compounds in the binding pocket (i.e., by substituting the number of contacts of each docked compound into the regression equation corresponding to the dbCICA model). Well-behaved potent compounds were retained in the binding pocket for subsequent manipulation (here, "well-behaved" compounds are defined as training compounds with bioactivities that are accurately predicted by the selected optimal dbCICA model; i.e., there was a relatively small residual difference between the fitted and experimental bioactivities as predicted by the particular dbCICA

Table 1 Highest-ranking anti-Hsp90α dbCICA models, their corresponding parameters, and statistical criteria

dbCICA model	Ligand ionization state	Explicit water[a]	Scoring function	Contact distance threshold[b] (Å)	Number of positive contacts[c]	Number of negative contacts[d]	r_{83}[e]	r^2_{LOO}[f]	$r^2_{5\text{-fold}}$[g]
I	Ionized	Present	JAIN	3.5	8	10	0.75	0.54	0.54
II	Unionized	Present	JAIN	3.5	8	5	0.81	0.64	0.66
III	Unionized	Present	PLP2	3.5	5	5	0.81	0.63	0.64

[a] Crystallographically explicit water of hydration. [b] Distance thresholds used to define ligand–binding site contacts. [c] Optimal number of combined (i.e., summed) bioactivity-enhancing ligand–binding site contacts. [d] Optimal number of combined (i.e., summed) bioactivity-disfavoring ligand–binding site contacts. [e] Non-cross-validated correlation coefficient for 83 training compounds. [f] Cross-validation correlation coefficients determined by the leave-one-out technique. [g] Cross-validation correlation coefficients determined by the leave-one-out technique repeated five times

Table 2 Critical binding-site contact atoms proposed by the optimal dbCICA models for Hsp90α inhibitors

dbCICA model	Favored contact atoms (positive contacts)[a,b]		Disfavored contact atoms (negative contacts)[e]
	Amino acids and corresponding atom identities [c]	Weights[d]	
I	ASP102: OD2	2	ASN51:HB1, ASP54:HA, ASP93:CG, ASP93:OD1, GLY97:HA1, LEU107:CD1, LYS112:HD1, MET98:SD, HOH106:H2, HOH132:H1
	ASP54:OD1	3	
	ILE96:CB	2	
	ILE96:HG11	3	
	PHE138:CE1	3	
	TYR139:CZ	2	
	HOH141:H2	3	
	HOH188:H2	1	
II	ASN51:HD22	3	ALA55:N, ASN51:OD1, ASP93:CG, SER52:OG, TYR139:CD2
	ASP102:OD2	3	
	HIS154:ND1	1	
	LYS112:HZ3	2	
	LYS58:HE1	2	
	THR184:HG21	1	
	THR184:OG1	2	
	HOH246:O	2	
III	THR184:HG1	2	ALA55:HA, ASN51:HA, ASN51:O, GLY97:CA, SER52:CA
	VAL136:O	2	
	THR184:HG22	1	
	ASP102:OD1	2	
	LYS112:HZ1	1	

[a] Numbers and distance thresholds are as in Table 1. [b] Bioactivity-enhancing ligand–binding-site contacts. [c] Binding-site amino acids and their significant atomic contacts. Atom codes are as provided by the Protein Data Bank file format [e.g., ASP102:OD2 encodes for an oxygen atom (D2) of the carboxylic acid side chain of aspartic acid 102], except for hydrogen atoms, which were coded by DS 2.5. [d] Degree of significance (weight) of the corresponding contact atom, which indicates the number of times it emerges in the final dbCICA model [see point (iii) in the section "Docking-based comparative molecular contacts analysis (dbCICA)" under "Experimental"). [e] Bioactivity-disfavoring ligand–binding-site contacts (steric clashes)

model; see Figs. 2, 3, 4, and 5). Badly predicted docked compounds were discarded.

3. Significant positive contacts in the binding pocket (i.e., those that have weights of 2 or 3) were marked and carefully assessed to identify their closest ligands' moieties. Consensus among potent, well-behaved training compounds that moieties with the same physicochemical properties should be positioned adjacent to a significant contact atom in the binding pocket (as defined by the dbCICA model) warranted the placement of the corresponding pharmacophoric feature into that region. For example, if potent, well-behaved docked compounds agreed that quaternary ammonium moieties should be placed adjacent to a certain dbCICA significant contact point [within the predefined distance threshold, see point (i) in the section "Docking-based comparative molecular contacts analysis (dbCICA)" under "Experimental"], then a positive ionizable (PosIon) feature was placed on top of the quaternary ammonium moieties. The pharmacophoric query features were added manually from the DS 2.5 feature library, and the default feature radius (1.6 Å) was employed.
4. Finally, to account for the steric constraints of the binding pocket, binding-site atoms that exhibited contacts that were negative correlated with bioactivity [i.e., those inverted in step (ii) in the section "Docking-based comparative molecular contacts analysis (dbCICA)" under "Experimental"] were marked and used as centers for exclusion spheres. Negative contacts identify spaces that are occupied by docked conformers/poses of inactive compounds and are free of active ones, so they can be filled with exclusion volumes. Exclusion spheres were added manually from the DS 2.5 feature library, and the default feature radius (1.2 Å) was employed.

In silico screening of the NCI database for new Hsp90α inhibitors

The resulting pharmacophore models (Hypo-IA, Hypo-IB, Hypo-II, and Hypo-III) were further sterically refined by adding exclusion volumes via the software package HipHop-Refine [80–82] (part of the Catalyst software suite from Accelrys Inc.); see the section "SM-2" and Table C in the ESM for more experimental details. The sterically refined versions of the four pharmacophores were employed as 3D search queries to screen the National Cancer Institute (NCI) list of compounds (238,819 compounds). Screening was performed employing the "best flexible database search" option implemented within Catalyst.

NCI hits were subsequently filtered based on molecular weight, such that only hits with molecular weights of ≤550

Daltons were retained. Surviving hits were docked into the ATPase-binding pocket of Hsp90α (PDB code: 1YET, resolution 1.9 Å), employing the docking conditions of the corresponding successful dbCICA models (models I, II, or III, Table 1 and 2). The resulting docked poses were subsequently analyzed for critical contacts according to the dbCICA models I, II, or III (Table 1 and 2), and the number of critical contacts for each hit compound was used to rank the hits. The highest-ranking available hits were acquired and tested in vitro.

In vitro experimental studies

Materials

NCI samples were kindly provided by the National Cancer Institute and were of purity >95 %. Recombinant human Hsp90α (Bioquote, York, UK), ATP 100X solution, geldanamycin standard inhibitor (Bioquote), a Quantichrome ATPase/GTPase kit (BioAssay Systems, Hayward, CA, USA), water for bioanalysis (Sigma, St. Louis, MO, USA), and DMSO for bioanalysis (Sigma) were also used.

Preparation of hit compounds for in vitro assay

The tested compounds were provided as dry powders in variable quantities (30 mg). They were initially dissolved in DMSO to give stock solutions of 0.20 M. Subsequently, they were diluted to the required concentrations with deionized water for enzymatic assay.

Quantification of the inhibitory effect on Hsp90α using a spectrophotometric assay

The ATPase activity of Hsp90α was quantified by colorimetric measurement of released inorganic phosphate. Bioassays were performed by mixing Hsp90α solution (6 μL, 25 μg/mL in assay buffer), 24 μL of assay buffer, and 5 μL of the particular tested compounds to yield final inhibitor concentrations of 10, 1, and 0.1 μM per well (in some cases 0.01 μM). The final concentration of DMSO did not exceed 1.0 %. The mixtures were incubated for 30 min at 37 °C in an ELISA plate shaker, and then ATP solutions (5 μL, 4 mM in assay buffer) were added to each mixture. A blank was prepared as above except that 5 μL of distilled water were used instead of inhibitor solution. The mixtures were equilibrated to 37 °C and incubated for 24 h.

The enzymatic reaction was terminated by the addition of 80 μL of malachite green ammonium molybdate–Tween 20 solution in 0.27 M H_2SO_4 and 10 μL of 34 % sodium citrate. Color was allowed to develop at room temperature for 30 min, and sample absorbances were determined at λ_{max}=620 nm using a plate reader (ELx 800, BioTek Instruments, Winooski, VT, USA). Inhibition of Hsp90α was calculated as the percent activity of the uninhibited ATPase control. Geldanamycin was tested as a positive control, while negative controls were prepared by adding the substrate after reaction termination [83–85].

Results and discussion

Basic concept of dbCICA

Although docking engines suffer from an inability to calculate the free energy of binding, they normally succeed in reproducing co-crystallized ligand poses/conformations among their high-ranking docking solutions [38, 52–56]. This suggests that it is quite possible to correlate docked 3D ligand poses/conformers with bioactivities, as shown previously using CoMFA modeling [58, 72, 73].

In dbCICA, interest is focused on identifying a set of atoms within the binding site that tend to contact with potent docked ligands and avoid poorly active docked ligands. If such a set of contact atoms is identified for a docked list of ligands, then one can assume that the docking configuration is successful (i.e., it succeeded in arranging the molecules in a such way that explains the variation in bioactivity).

Presumably, high ligand–receptor affinity is mediated by a certain critical number of interactions; i.e., potent ligands usually participate in certain critical interactions (hotspots) within the binding pocket. However, the fact that docking engines and scoring functions evaluate a large number of ligand–receptor interactions to generate their docking solutions means that the influence of these critical interactions could be diluted or even overlooked. In this context, identifying a set of affinity-discriminating contact atoms within the binding site should help us to not only validate a particular docking configuration but also to pinpoint the critical ligand–receptor interactions that are responsible for affinity, as these discriminatory contacts encode for nearby attractive interactions. In fact, the resulting dbCICA models can be translated into pharmacophoric models with a limited number of critical binding features, which can then be used as 3D search queries to mine for new ligands.

Practical aspects and the implementation of dbCICA

The dbCICA concept prompts a question about the definition of "contacts"—the interatomic distance thresholds that can be considered acceptable contacts. The fact that most ligand–receptor interactions, including hydrogen bonding and van der Waals forces, show their optimal strengths at distances of 2.0–3.5 Å prompted us to perform dbCICA analysis by implementing three distance thresholds as interatomic contacts: 2.0, 2.5, or 3.5 Å. Interatomic distances below (or equal

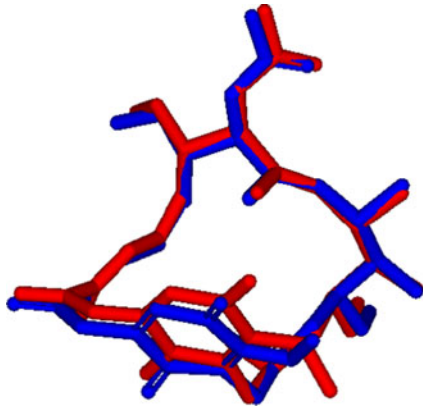

Fig. 1 Comparison between the co-crystallized pose of GMD (*red*, PDB code: 1YET, resolution 1.9 Å) and its docked pose in Hsp90α according to the docking conditions of models I, II, and III, showing an RMSD of 0.539 Å (*blue*, Table 1)

to) the predefined threshold are considered contacts and are encoded by a binary value of 1, while larger distances are considered noncontacts and encoded by a 0 (zero). Interatomic distances are calculated based on explicit hydrogen atoms.

As mentioned earlier, discriminatory ligand–receptor contacts are surrogates for nearby critical ligand–receptor interactions. However, since ligand–receptor affinity is normally mediated by a set of concomitant critical attractive interactions, it is expected that their proxy contacts are also concomitant. This basic principle is represented in dbCICA analysis by searching for discriminatory ligand–receptor contacts that have summation values that are directly proportional to bioactivity (i.e., searching for concurrent contacts rather than separate contacts).

Furthermore, in our dbCICA algorithm, there is the option to allow any particular positive contact column to emerge up to three times in the optimal summation model (i.e., allowing variable weights for contacts). This option identifies intermolecular contacts with higher weights or contributions in the optimal dbCICA models [see point (iii) in the section "Docking-based comparative molecular contacts analysis (dbCICA)" in "Experimental"].

Still, some contacts are expected to be inversely proportional to bioactivity (i.e., negative contacts). These contacts encode for repulsive interactions (steric clashes). However, to remove any correlation faults resulting from summations

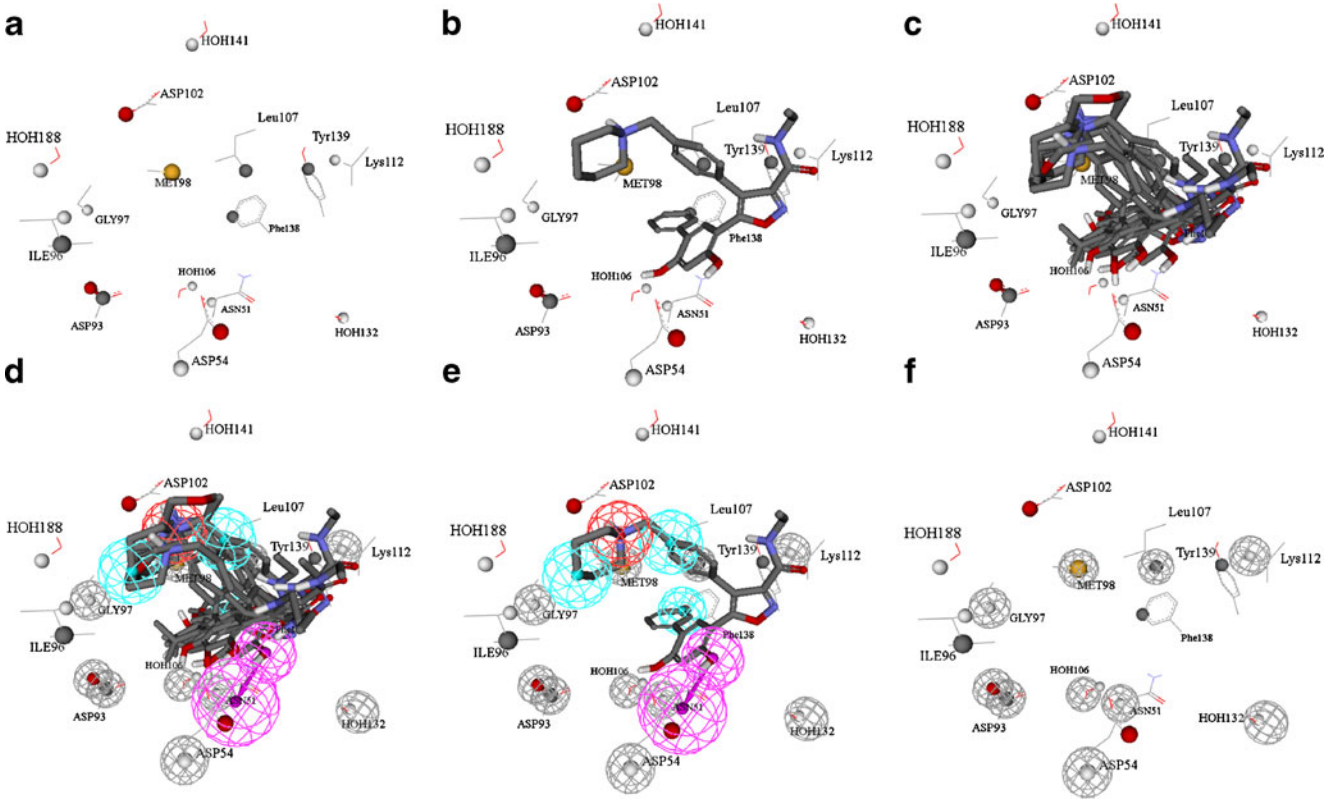

Fig. 2 Steps for the manual generation of the binding hypothesis Hypo-IA as guided by dbCICA model I (Tables 1 and 2). **a** The binding-site moieties in dbCICA model I, with significant contact atoms shown as *spheres*. **b** The docked pose of the well-behaved compound **40** (Fig. 1 and Table A in the ESM, IC_{50}=0.014 μM) within the binding pocket. **c** The docked poses of the well-behaved and potent compounds **38**, **40**, **43**, **44**, and **45** (Fig. 1 and Table A in the ESM). **d** Manually placed pharmacophoric features on chemical moieties common to the docked well-behaved potent compounds **38**, **40**, **43**, **44**, and **45**. *Light blue spheres* represent hydrophobic features, *red spheres* represent positive ionizable features, *violet spheres* represent hydrogen-bond donors, and *gray spheres* represent exclusion regions. **e** The docked pose of **40** and how it relates to the proposed pharmacophoric features. **f** Exclusion spheres fitted against binding-site atoms showing negative correlations with bioactivity (as emergent in dbCICA model I)

of negative and positive contacts during the search for optimal contact combinations, dbCICA analysis is preceded by a scan for the correlations between each contact column and bioactivity. Inversely proportional contacts (i.e., negative contacts) are removed during the initial search phase for optimal combinations of positive contacts.

Nevertheless, since ligand–receptor binding is controlled by both attractive and repulsive forces, both positive and negative contacts are later combined in dbCICA models. However, to maintain the consistency of correlation calculations (i.e., to maintain the trend for direct proportionality between the contact combinations and bioactivities), it was decided to invert the negative contacts by converting their zeros to ones and vice versa. Subsequently, a second search phase is performed to find optimal summations of negative contacts that, upon combination with previously defined optimal positive contact summations, yield optimal correlations with bioactivity.

It remains to be mentioned that dbCICA contact summation models are judged based on three success criteria: the correlation coefficient (r^2), the leave-one-out r^2 (r_{LOO}^2), or the K-fold r^2 ($r_{K\text{-fold}}^2$). See the section "Implementation of the genetic algorithm during dbCICA modeling" in "Experimental" for more details.

Using dbCICA to discover Hsp90α inhibitors

We decided to employ dbCICA to identify the optimal conditions and parameters needed for the successful docking of 83 Hsp90α inhibitors (Fig. A and Table A in the ESM). The optimal dbCICA models were converted into pharmacophore hypotheses, which we used as 3D search queries to mine for new ATPase inhibitors of Hsp90α from the NCI list of compounds.

The study was performed as follows. The collected compounds were docked into the ATPase active site of Hsp90α, employing the LigandFit docking engine [29, 74]. We selected the Hsp90 crystal structure (i.e., 1YET) of a relatively large binding pocket (i.e., compared to other related structures, e.g., 2VCI or 2VCJ or 2UWD) to allow the docking engine to explore diverse docked ligand poses/conformers,

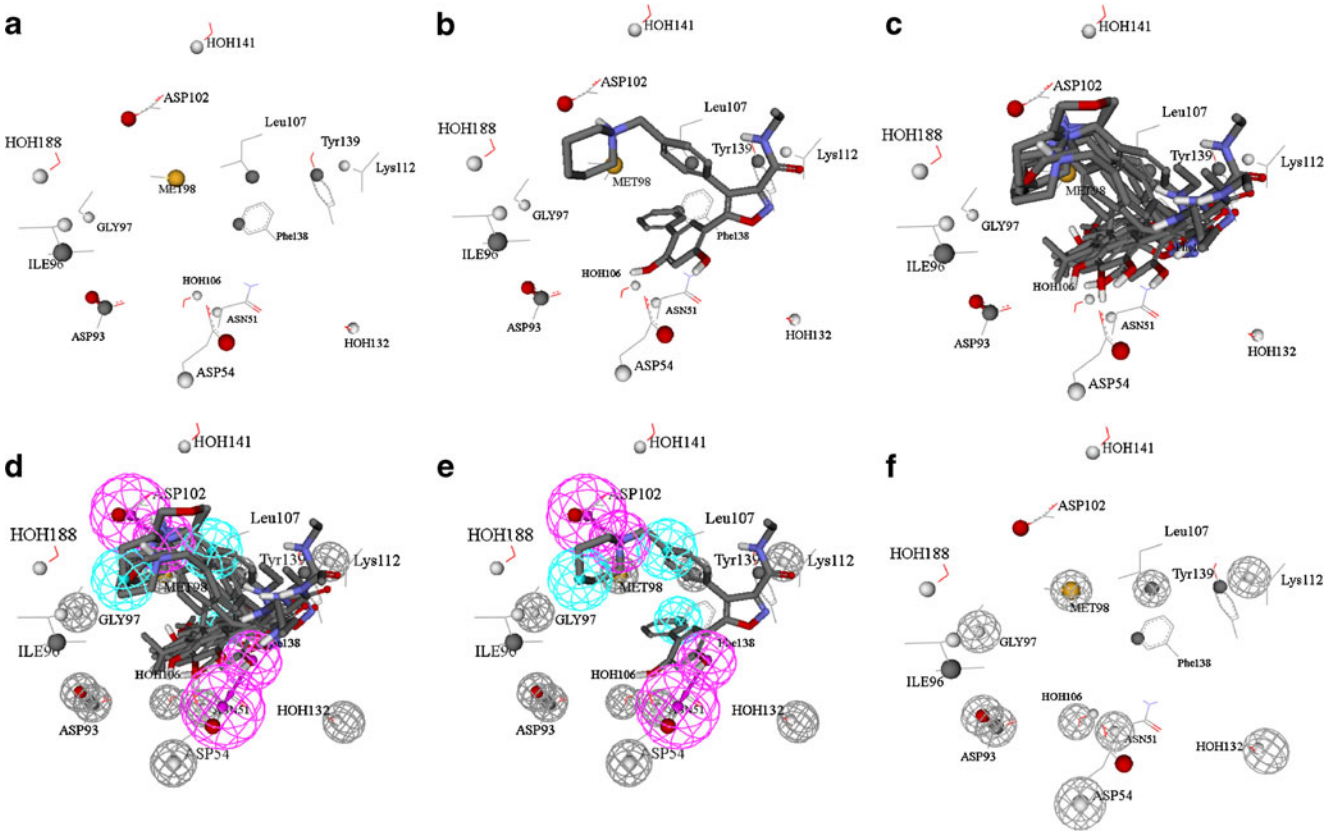

Fig. 3 Steps for the manual generation of the binding hypothesis Hypo-IB as guided by dbCICA model I (Tables 1 and 2). **a** The binding-site moieties in dbCICA model I, with significant contact atoms shown as *spheres*. **b** The docked pose of the well-behaved compound **40** (Fig. 1 and Table A in the ESM, IC_{50}=0.014 μM) within the binding pocket. **c** The docked poses of the well-behaved and potent compounds **38**, **40**, **43**, **44**, and **45** (Fig. 1 and Table A in the ESM). **d** Manually placed pharmacophoric features on chemical moieties common to the docked well-behaved potent compounds **38**, **40**, **43**, **44**, and **45**. *Light blue spheres* represent hydrophobic features, *violet spheres* represent hydrogen-bond donors, and *gray spheres* represent exclusion regions. **e** The docked pose of **40** and how it relates to the proposed pharmacophoric features. **f** Exclusion spheres fitted against binding-site atoms showing negative correlations with bioactivity (as emergent in dbCICA model I)

thus leading to a better test of the ability of dbCICA analysis to identify the best docking solutions. This is particularly important since the training compounds are closely congeneric, which might lead different docking settings to converge on closely related docked poses/conformers.

Four docking variations were implemented: two related to ligand ionization (ionized vs. unionized ligands), and two related to the binding site hydration state (a hydrated vs. a nonhydrated binding site).

Subsequently, the resulting docking solutions were scored by six different scoring functions: Jain [41], LigScore1, LigScore2 [34, 74], PLP1 [79], PLP2 [45], and PMF [49, 51]. The highest-ranking ligand conformers/poses, based on each scoring function, were aligned against each other to construct the corresponding dbCICA models.

Three contact binary matrices were generated for each docking-scoring solution (see the section "Docking-based comparative molecular contacts analysis (dbCICA)" in "Experimental"). Subsequently, a genetic algorithm (GA)-based search was implemented to search for the best combination (summation) of ligand–receptor intermolecular contacts capable of explaining the variation in bioactivity across the training compounds. GA was instructed to scan combinations of 2–10 directly proportional intermolecular (positive) contacts, followed by five or ten inversely proportional (negative) contacts.

Table 1 shows the contacts thresholds in Å, the number of positive and negative contacts, and statistical criteria for the three best dbCICA models. In the table, it is clear that all high-ranking dbCICA models have mediocre statistical criteria, with $r_{5\text{-fold}}^2$ values ranging from 0.54 to 0.66. We believe that this behavior is due to the fact that, in dbCICA modeling, the bioactivities of training compounds are correlated with contact summation (i.e., a single descriptor in each round of genetic iterations). Correlation with a single descriptor is expected to yield mediocre correlation statistics. However, correlation with multiple contacts failed to achieve any substantial prediction. Moreover, the fundamental theory of dbCICA is based on the occurrence of simultaneous contacts, which are best represented by summation. Therefore, we believe that the best use of dbCICA statistical criteria is to rank the corresponding models and prioritize them for translation into pharmacophore models.

Table 1 shows that JAIN-based scoring was superior to other scoring functions, as two out of the three best dbCICA models were based on JAIN, followed by the PLP2

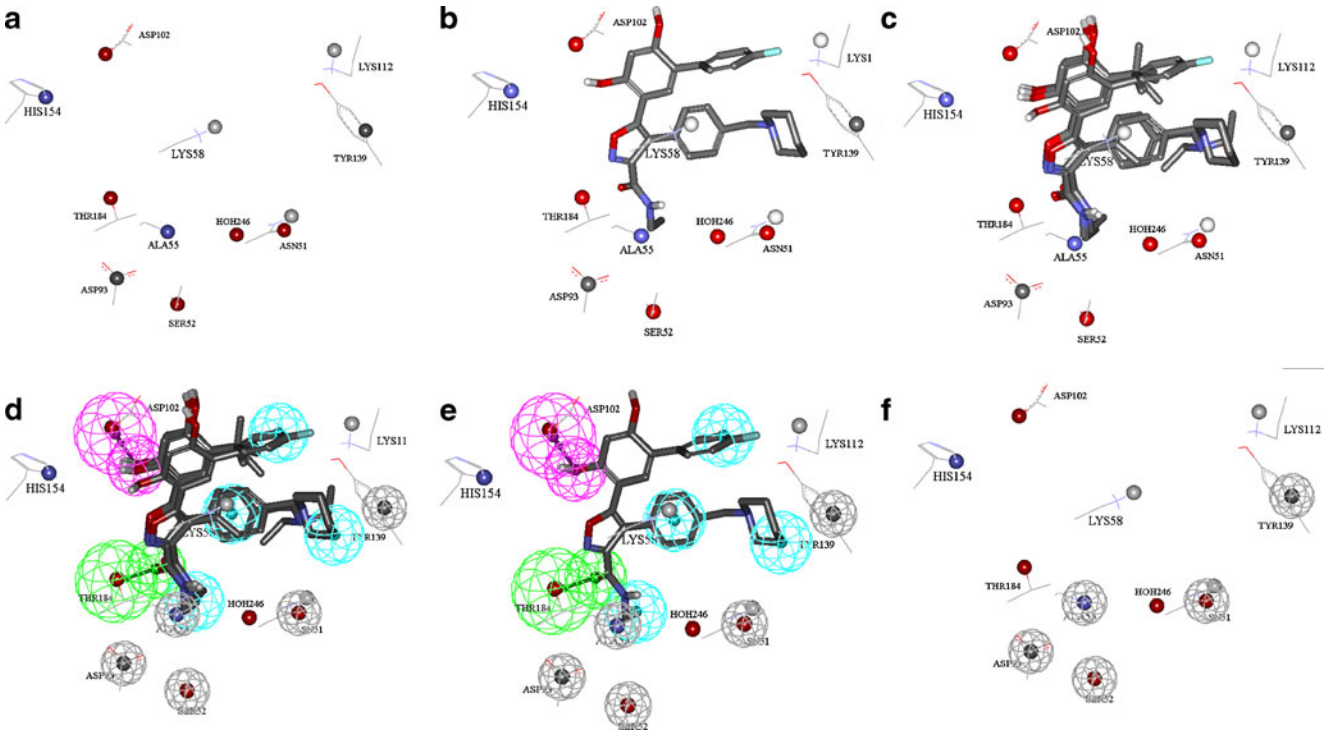

Fig. 4 Steps for the manual generation of the binding hypothesis Hypo-II as guided by dbCICA model II (Tables 1 and 2). **a** The binding-site moieties in dbCICA model II, with significant contact atoms shown as *spheres*. **b** The docked pose of the well-behaved compound **42** (Fig. 1 and Table A in the ESM, IC_{50}=0.036 μM) within the binding pocket. **c** The docked poses of the well-behaved and potent compounds **34**, **40**, **42**, **43**, **44** and **45** (Fig. 1 and Table A in the ESM). **d** Manually placed pharmacophoric features on chemical moieties common to the docked well-behaved potent compounds **34**, **40**, **42**, **43**, **44**, and **45**. *Light blue spheres* represent hydrophobic features, *violet spheres* represent hydrogen-bond donors, *green spheres* represent hydrogen-bond acceptors, and *gray spheres* represent exclusion regions. **e** The docked pose of **42** and how it relates to the proposed pharmacophoric features. **f** Exclusion spheres fitted against binding-site atoms showing negative correlations with bioactivity (as emergent in dbCICA model II)

scoring function. Similarly, a hydrated binding pocket enhanced the quality of the dbCICA models, as all high-ranking dbCICA models were based on docking solutions performed on a hydrated binding pocket. However, ligand ionization seems to be less important, as only one out of the three successful dbCICA models was based on ionized ligands, (i.e., dbCICA model I, Table 1). Each of the three optimal dbCICA models in Table 1 provided an excellent framework for subsequent development into a promising pharmacophoric hypothesis for in silico screening (see below). Interestingly, the docking conditions corresponding to the three optimal dbCICA models succeeded in reproducing the co-crystallized conformer of geldanamycin. In fact, the three docking conditions yielded almost the same geldanamycin docked conformer/pose close to the co-crystallized conformer (RMS=0.539 Å; see the section "Validation of optimal anti-Hsp90α dbCICA models" in "Results and discussion" for more details). Figure 1 compares how these conditions dock geldanamycin in comparison to the corresponding co-crystallized structure.

Figures 2, 3, 4, and 5 show the critical contact atoms within the Hsp90α binding site, while Table 2 lists them and their weights as proposed by the optimal dbCICA models I, II, and III. It is apparent from the table and figures that, despite their consensus in reproducing the same docked conformer/pose for geldanamycin (Fig. 1), the three optimal dbCICA models point to different binding modes for different ligands within the Hsp90α binding pocket. However, the repeated emergence of ASP102 in the three optimal models (Table 2) strongly suggests that this amino acid plays a central role in ligand–Hsp90α binding. The significance of this amino acid in ligand–Hsp90α binding has also been highlighted in previous publications [82, 83, 86].

Figures 2 and 3 show how dbCICA model I was translated into the corresponding pharmacophoric models Hypo-IA and Hypo-IB employing the DS 2.5 environment. Initially, the binding pocket was annotated by rendering significant contact atoms that had emerged in dbCICA model I into spherical forms (see Figs. 2a and 3a). Subsequently, we selected a few potent (IC_{50}< 0.05 μM) and well-behaved docked compounds (i.e., which showed the smallest differences between experimental and fitted bioactivities, as determined by regressing the inhibitors' bioactivities and their docking-based contact summations). Thereafter, appropriate pharmacophoric features were placed onto chemical functionalities common to the aligned docked compounds, as shown in Figs. 2d and 3d (see the section "Generation of

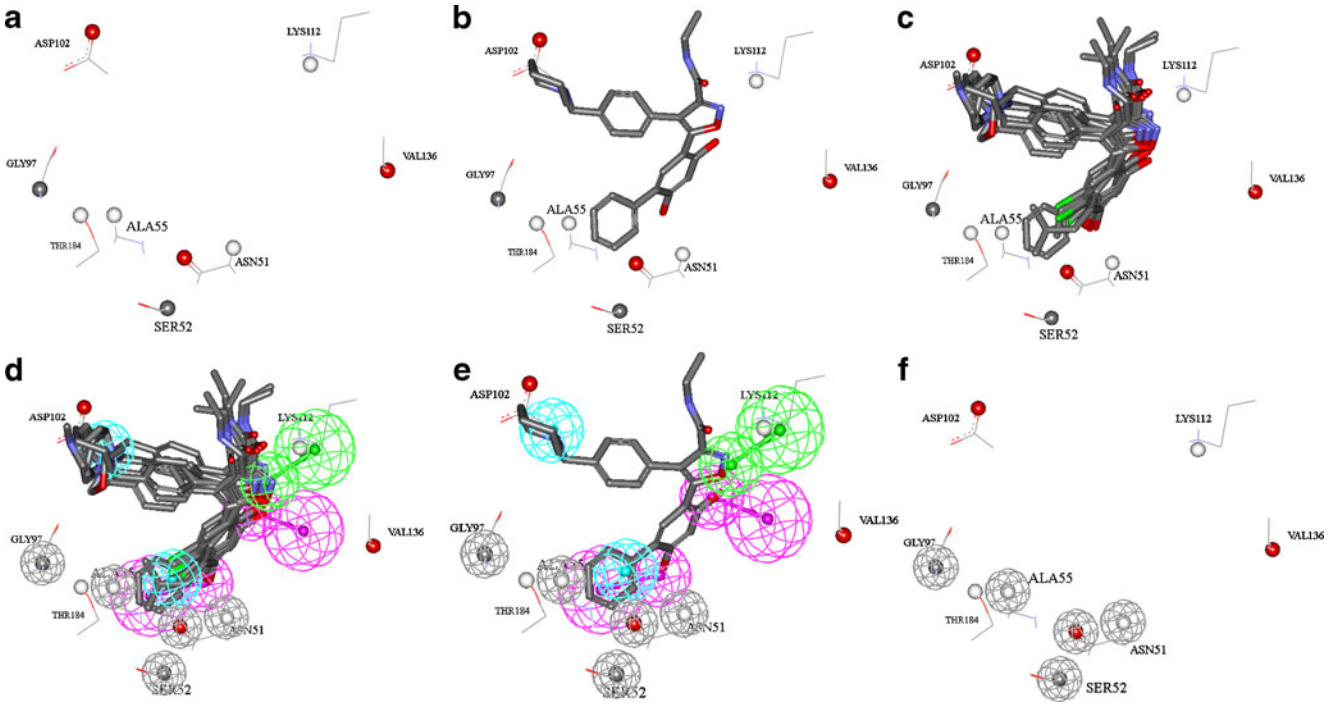

Fig. 5 Steps for the manual generation of the binding hypothesis Hypo-III as guided by dbCICA model III (Tables 1 and 2). **a** The binding-site moieties in dbCICA model A-III, with significant contact atoms shown as *spheres*. **b** The docked pose of the well-behaved compound **40** (Fig. 1 and Table A in the ESM, IC_{50}=0.014 μM) within the binding pocket. **c** The docked poses of the well-behaved and potent compounds **20**, **23**, **25**, **26**, **36**, **40**, and **48** (Fig. 1 and Table A in the ESM). **d** Manually placed pharmacophoric features on chemical moieties common to the docked well-behaved potent compounds **20**, **23**, **25**, **26**, **36**, **40**, and **48**. *Light blue spheres* represent hydrophobic features, *violet spheres* represent hydrogen-bond donors, *green spheres* represent hydrogen-bond acceptors, and *gray spheres* represent exclusion regions. **e** The docked pose of **40** and how it relates to the proposed pharmacophoric features. **f** Exclusion spheres fitted against binding-site atoms showing negative correlations with bioactivity (as emergent in dbCICA model III)

Table 3 The statistical results for the CoMFA models obtained via high-ranking anti-Hsp90α dbCICA-based docking/scoring combinations (as in Table 1)

dbCICA models[a]		Docking conditions[a]	Scoring function[a]	Terms[b]	PC[c]	Statistical criteria			
						r^2 [d]	r^2_{LOO} [e]	r^2_{BS} [f]	r^2_{PRESS} [g]
Highest[h] ranking	I	LigandFit; ionized ligands;hydrated binding pocket	JAIN	16	3	0.89	0.77	0.86	0.304 (0.49)[i]
	II	LigandFit; unionized ligands; hydrated binding pocket	JAIN	16	4	0.91	0.81	0.88	0.36[j] (0.48)
	III	LigandFit; unionized ligands; hydrated binding pocket	PLP2	8	4	0.77	0.66	0.76	0.384[k] (0.623)
Lowest[l] ranking		LigandFit; ionized ligands; nonhydrated binding pocket	PMF	6	5	0.68	0.60	0.66	−1.6

[a] dbCICA models and corresponding docking/scoring conditions are as described in Table 1

[b] Number of descriptor terms in the best CoMFA model

[c] Number of principal components (latent variables) in the best CoMFA model

[d] Non-cross-validated correlation coefficient for 67 training compounds

[e] Cross-validation correlation coefficients determined by the leave-one-out technique

[f] Bootstrapping correlation coefficient

[g] Predictive r^2 determined for the 16 test compounds

[h] dbCICA models numbered as in Table 1

[i] r_{PRESS}^2 value after removing one outlier, i.e., compound **50**

[j] r_{PRESS}^2 value after removing one outlier, i.e., compound **64**

[k] r_{PRESS}^2 value after removing one outlier, i.e., compound **73** (see Table A in the ESM for the structures of outliers)

[l] Example of a low-ranking dbCICA model (data not shown)

pharmacophores corresponding to successful dbCICA models" under "Experimental" for more details).

The pharmacophoric features were placed in such a way as to highlight the interactions encoded by the nearest critical contacts. For example, in the case of dbCICA model I, the emergence of a significant contact at the carboxylic oxygen of Asp102, combined with the consensus among well-behaved, potent docked ligands that quaternary ammonium groups

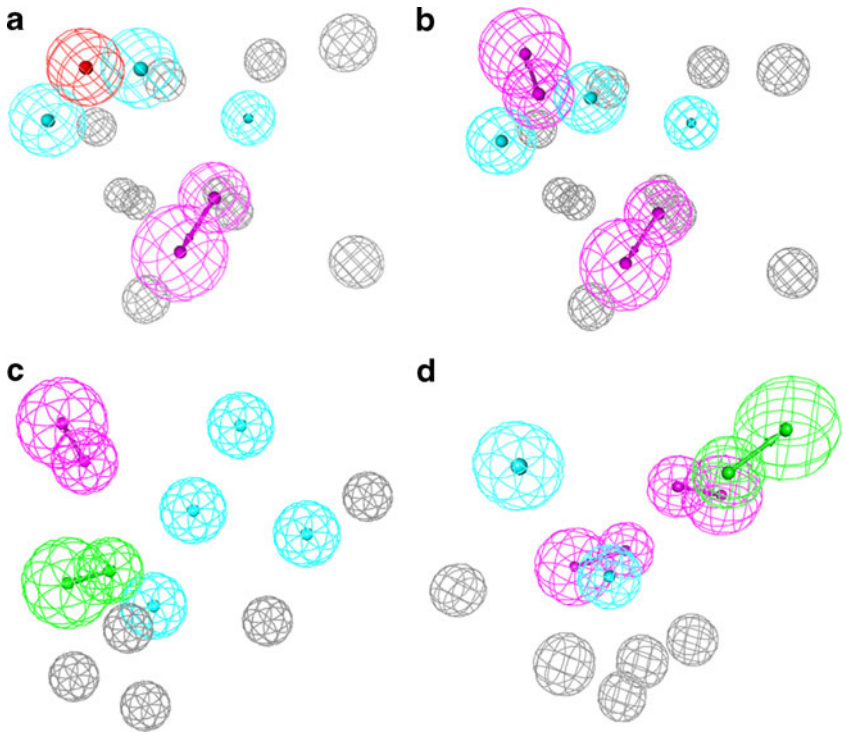

Fig. 6 Pharmacophoric features and exclusion spheres of **a** Hypo-IA, **b** Hypo-IB, **c** Hypo-II, and **d** Hypo-III. *Light blue spheres* represent hydrophobic features, *red spheres* represent positive ionizable features, *violet spheres* represent hydrogen-bond donors, *green spheres* represent hydrogen-bond acceptors, and *gray spheres* represent exclusion regions

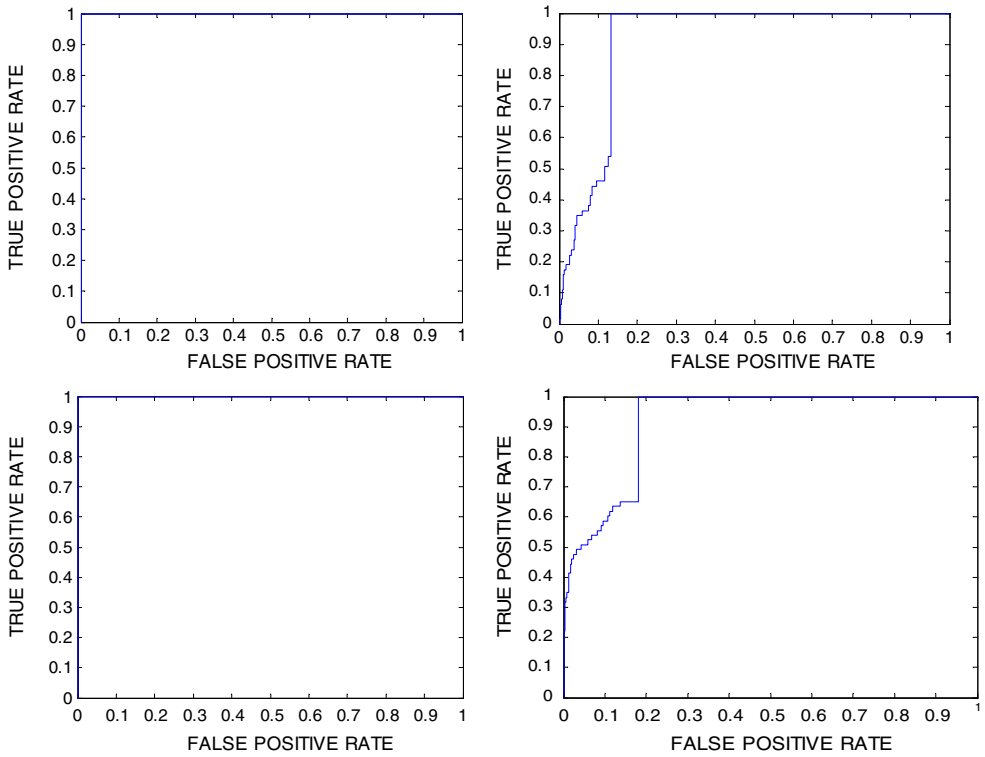

Fig. 7 Receiver operating characteristic (ROC) curves for dbCICA-based pharmacophores: **a** Hypo-IA, **b** Hypo-IB, **c** Hypo-II, and **d** Hypo-III

should be placed nearby (Figs. 2c and 3c), prompted us to place a positive ionizable feature on the ammonium groups in Hypo-IA (Fig. 2d). However, to account for the possibility that the ligands' quaternary ammonium groups interact with Asp102 via hydrogen-bonding interactions, we suggested placing a hydrogen-bond donor (HBD) feature at the same position in a second related pharmacophore model derived from dbCICA model I: Hypo-1B (Fig. 3; note that Hypo-1A and Hypo-1B are identical in all other features.

Similarly, agreement among the docked, potent, and well-behaved inhibitors that hydrophobic moieties should be placed adjacent to PHE138 (carbon CE1), ILE96 (CB and HG11), and H_2O141 prompted us to place hydrophobic pharmacophoric features at these positions, as shown in Figs. 2d and e (or Figs. 3d and e). Finally, the significant dbCICA contact at the carboxylic oxygen of ASP54 apparently encodes for hydrogen bonding with hydrogen-bond donors at the ligand side. This conclusion is supported by the consensus among docked ligands that hydrogen-bond donors should be oriented towards the ASP54 carboxylic acid. Accordingly, we were prompted to direct the HBD feature towards the carboxylic acid side chain of ASP54.

A similar strategy was implemented for the development of pharmacophore models Hypo-II and Hypo-III, starting from dbCICA models II and III, respectively (Tables 1 and 2). Figures 4 and 5 show how these pharmacophore models—including their exclusion regions—were generated, while Table B in the ESM shows the *x*, *y*, and *z* coordinates of the generated pharmacophores.

Table 4 ROC curve analysis criteria for dbCICA-selected pharmacophores

Pharmacophore model	ROC[a]-AUC[b]	ACC[c]	SPC[d]	TPR[e]	FNR[f]
Hypo-IA	1.0	0.926	0.953	0.587	0.046
Hypo-IB	0.913	0.926	0.957	0.539	0.043
Hypo-II	1.0	0.926	0.921	1.0	0.079
Hypo-III	0.919	0.927	0.949	0.65	0.05

[a] *ROC* receiver operating characteristic curve

[b] *AUC* area under the curve

[c] *ACC* overall accuracy

[d] *SPC* overall specificity

[e] *TPR* overall true positive rate

[f] *FNR* overall false negative rate

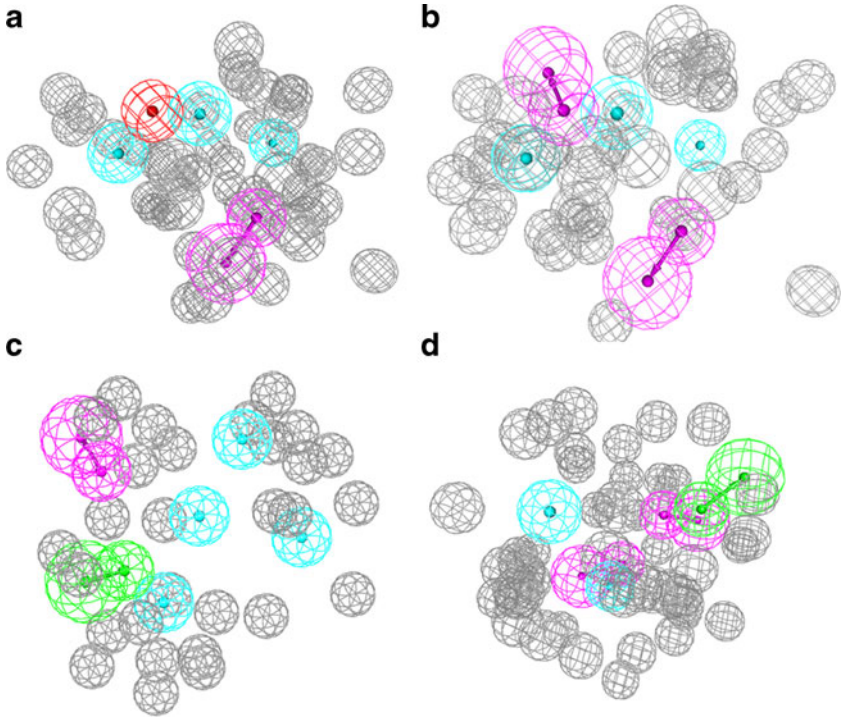

Fig. 8 Sterically refined versions of **a** Hypo-IA (39 added exclusion spheres), **b** Hypo-IB (29 added exclusion spheres), **c** Hypo-II (24 added exclusion spheres), and **d** Hypo-III (43 added exclusion spheres)

Validation of the optimal anti-Hsp90α dbCICA models

Three validation procedures were implemented to assess the dbCICA models: self-docking, CoMFA, and ROC analyses.

1. *Self-docking*. To assess the similarity between the ligand poses/conformers produced by the docking conditions of dbCICA models I, II, and III (Table 1) and the crystallographic structure of the bound ligand, we compared the docked poses of geldanamycin obtained using the docking conditions of the three successful dbCICA models with its co-crystallized pose (PDB code: 1YET, resolution 1.9 Å). We compared our docking solutions with this particular Hsp90α complex because all of our docking–dbCICA modeling explorations were conducted using this protein template.

Figure 1 compares the docked poses against the co-crystallized pose. From the figure, it is clear that the three docking solutions are very similar to the experimental co-crystallized complex (RMS= 0.539 Å). Interestingly, the three docking conditions produced identical docking solutions for geldanamycin, despite their apparent differences from other ligands (see Figs. 2, 3, 4, and 5). Apparently, the

Table 5 Numbers of selected, filtered, tested, active, and inactive hits retrieved by Hypo-IA, Hypo-IB, Hypo-II, and Hypo-III from the NCI's list of compounds[a]

		Number of in silico hits retrieved by			
		Refined Hypo-IA	Refined Hypo-IB	Refined Hypo-II	Refined Hypo-III
Post-screening filtering[b]	Before	130	412	67	1855
	After	123	332	48	1345
Acquired from the NCI[c]		16	9	6	9
Number of actives[d]		9	6	4	3
Assayed to determine IC_{50}		6	4	4	2

[a] The National Cancer Institute's (NCI) list of available compounds includes 238,819 structures

[b] Using Lipinski's and Veber's rules. A maximum of two violations of Lipinski's rule were tolerated

[c] The total number of compounds acquired from the NCI was 40 compounds. These resemble the highest ranking compounds based on their fit values with respect to the corresponding pharmacophores

[d] Compounds with inhibition percentages of ≥25 % at 10 μM were considered actives. The total number of captured active compounds is 21, among which one compound (**89**, Fig. 9) was captured by both Hypo-IB and Hypo-III. See Table 6 for the pharmacophoric origins of each captured active compound

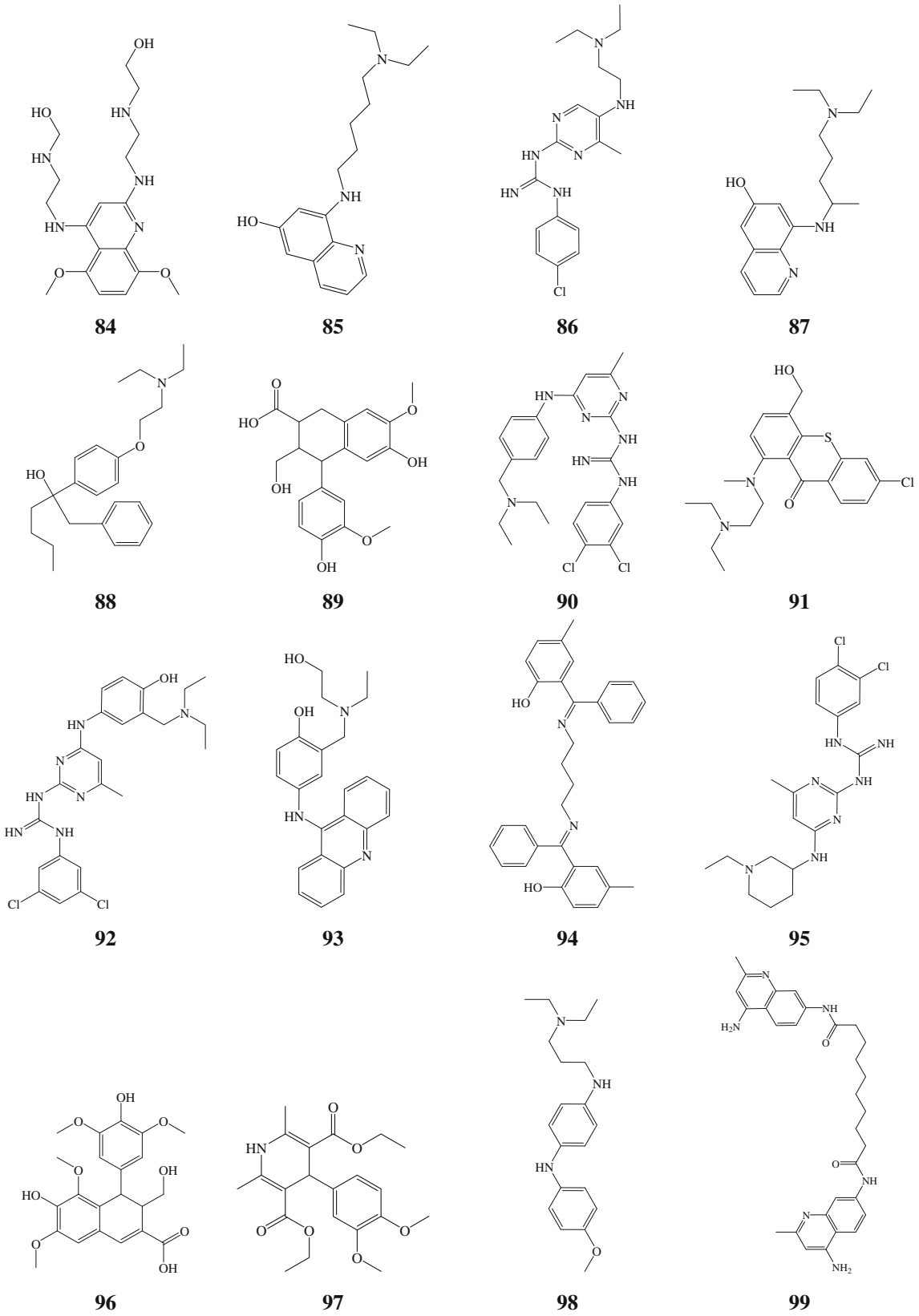

Fig. 9 Chemical structures of the tested highest-ranking hits captured by the dbCICA models (see Table 6 for the corresponding bioactivities)

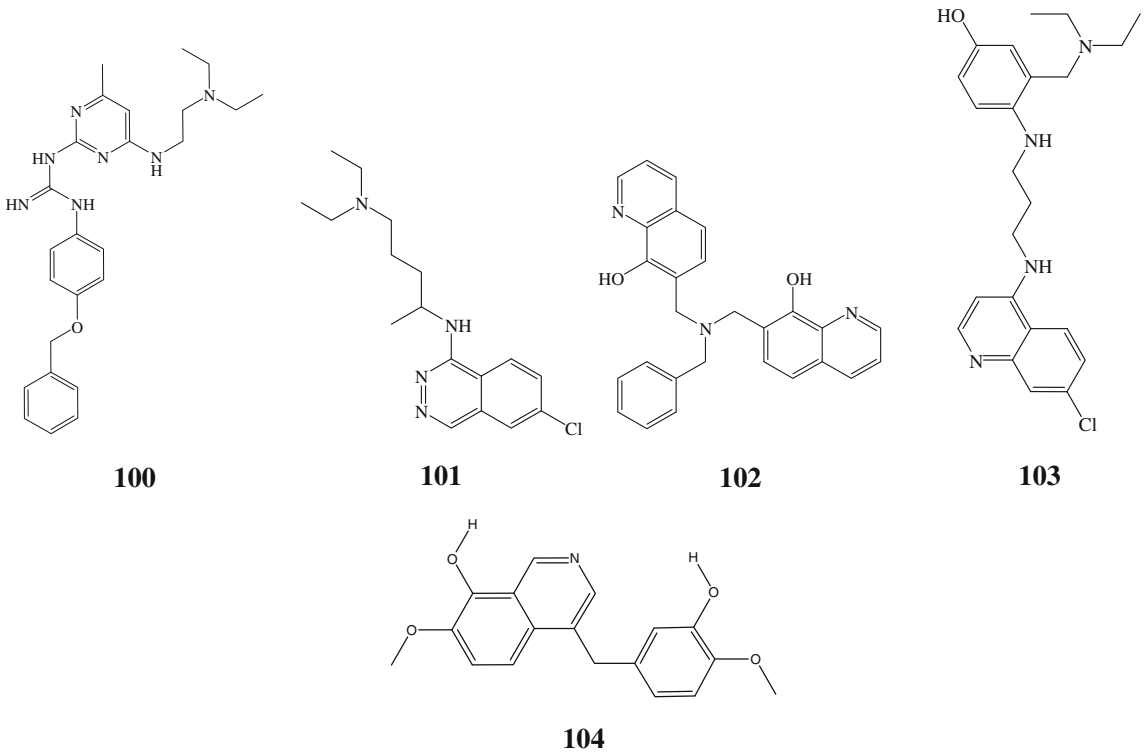

Fig. 9 (continued)

large molecular size and feature-rich nature of geldanamycin, combined with its rigid structure, force the three docking conditions to converge upon a single docked conformer/pose for geldanamycin.

Table 6 High-ranking NCI active hits captured by the dbCICA-based pharmacophores

Compound[a]	NCI code	Percent inhibition at 10 μM[b]	Pharmacophore[c]
84	NSC365362	79 %	Hypo-III
85	NSC56634	80 %	Hypo-IA
86	NSC5475	64 %	Hypo-IA
87	NSC55136	74 %	Hypo-IA
88	NSC63289	68 %	Hypo-IA
89	NSC32977	70 %	Hypo-IB, Hypo-III
90	NSC142539	65 %	Hypo-IB
91	NSC166380	55 %	Hypo-IA
92	NSC157531	59 %	Hypo-II
93	NSC12270	53 %	Hypo-II
94	NSC362149	56 %	Hypo-IB
95	NSC305761	52 %	Hypo-IA
96	NSC106052	48 %	Hypo-III
97	NSC282463	47 %	Hypo-II
98	NSC13617	44 %	Hypo-IA
99	NSC12150	48 %	Hypo-II
100	NSC141100	43 %	Hypo-IA
101	NSC56615	40 %	Hypo-IA
102	NSC130822	31 %	Hypo-IB
103	NSC146835	30 %	Hypo-IB
104	NSC131747	55 %	Hypo-IB

[a] Hits shown in Fig. 9

[b] Geldanamycin as the standard inhibitor with IC_{50}=420 nM. Reported Geldanamycin IC_{50}= 281 nM [95]. Corresponding dose–response relationships are shown in Fig. B in the ESM

[c] The pharmacophore(s) that was/were used to retrieve the hit

2. *CoMFA modeling*. To further validate our optimal dbCICA models (models I, II, and III; Table 1), we assessed whether their corresponding molecular alignments yield self-consistent and predictive CoMFA models [17, 58, 72, 73]. For comparison purposes, a similar assessment was performed for the molecular alignment of a low-ranking dbCICA model (e.g., docking ionized ligands into a nonhydrated binding pocket using the PMF scoring function, which achieved an $r_{5\text{-fold}}^2$ of 0.203; unpublished data). Table 3 shows the statistical criteria for the resulting CoMFA models.

   Table 3 shows that molecular alignments based on the top three dbCICA models (i.e., I, II, and III; Tables 1 and 2) achieved corresponding self-consistent CoMFA models of acceptable predictive power, particularly after eliminating one outlier from their testing sets. On the other hand, the low-ranking dbCICA model coincided with a low-quality CoMFA model that completely failed to predict the bioactivities of the testing set (negative r_{PRESS}^2 in Table 3). The good agreement between CoMFA and dbCICA provides additional evidence of the utility of dbCICA modeling as a validation technique in docking studies.

3. *Receiver operating characteristic curve analysis of corresponding pharmacophores* (Hypo-IA, Hypo-1B, Hypo-II, and Hypo-III; Fig. 6).

   The four pharmacophores were subjected to receiver operating characteristic (ROC) curve analysis. In ROC analysis, the ability of a particular pharmacophore model to correctly classify a list of compounds as actives or inactives is indicated by the area under the curve (AUC) of the corresponding ROC, as well as other parameters: overall accuracy, overall specificity, overall true positive rate, and overall false negative rate (see "SM-1" in the ESM for details) [70, 82, 87, 88–93]. Figure 7 and Table 4 show the ROC performances of our dbCICA-based pharmacophores. It is clear from both the figure and table that Hypo-IA and Hypo-II outperformed Hypo-IB and Hypo-III. The reason for this behavior is probably related to the presence of the positive ionizable feature in Hypo-IA and an extra feature in Hypo-II (six features compared to five in the other three pharmacophores). Positively charged atoms are relatively scarce, which enhances the selectivity of Hypo-IA, while the extra feature in Hypo-IB enforces additional 3D requirements on captured hits, thus boosting the selectivity of Hypo-II.

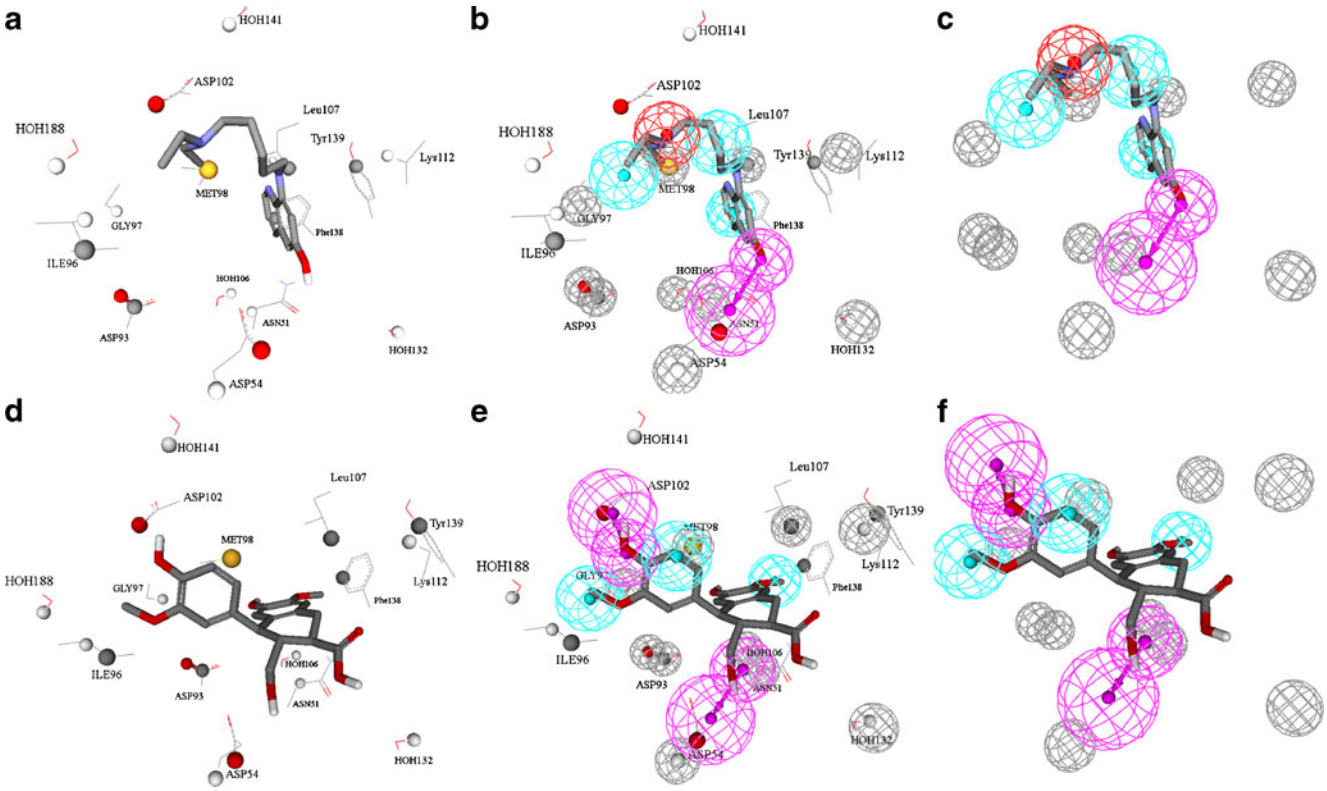

Fig. 10 Selected Hsp90α inhibitory hits and how they dock into the binding site of Hsp90. **a** The docked pose of hit **85** (Fig. 9 and Table 6, IC_{50}=4.6 μM), employing the docking conditions of model I (Tables 1 and 2). **b** The docked pose of **85** and how it relates to the pharmacophoric features of Hypo-IA. **c** Mapping the docked pose of **85** to Hypo-IA. **d** The docked pose of hit **89** (Fig. 9 and Table 6, IC_{50}=5.9 μM), employing the docking conditions of model I (Tables 1 and 2). **e** The docked pose of **89** and how it relates to the pharmacophoric features of Hypo-IB. **f** Mapping the docked pose of **89** to Hypo-IB

In silico screening and in vitro validation

Prior to in silico screening, we decided to sterically refine our dbCICA-derived pharmacophores in order to increase the probability of bioactivity in the captured hits. Steric refinement was performed by employing the HipHop-Refine module of the Catalyst package [80]. HipHop-Refine decorates pharmacophoric models with exclusion spheres that resemble sterically forbidden regions (i.e., sterically-clashing topologies within the binding pocket). HipHop-Refine requires a group of training compounds to identify spaces that are occupied by inactive compounds and are free from active ones, in order to fill them with exclusion volumes. See the section "SM-2" and Table C in the ESM for more information and experimental details about how we decorated our pharmacophores with additional exclusion spheres. Figure 8 shows the sterically refined versions of Hypo-IA, Hypo-IB, Hypo-II, and Hypo-III.

The sterically refined versions of the pharmacophores were implemented as 3D search queries to screen the National Cancer Institute's list of compounds (NCI; this includes 238,819 compounds). NCI hits were subsequently filtered by Lipinski's and Veber's rules [94]. The resulting hits were docked into the Hsp90α protein (PDB code: 1YET) employing the same docking conditions of dbCICA models I–III (as in Table 1) and fitted against the corresponding pharmacophores models. The fit values were employed to rank the corresponding hits and prioritize subsequent in vitro testing. The highest ranking 40 hits were acquired from the NCI and tested in vitro against Hsp90. Table 5 summarizes the number of hits retrieved using each pharmacophore and the remaining active hits following post-screen filtering and in vitro testing. Figure 9 shows the chemical structures of the active hits, while Table 6 shows their corresponding NCI codes, experimental bioactivity values, and the pharmacophores used to retrieve them. Figure B in the ESM shows the dose–response curves of the active hits.

Table 6 and Fig. 9 clearly show that out of the 40 highest-ranking hits acquired for experimental validation, 15 possessed significant ATPase inhibitory activities against Hsp90α (i.e., with inhibition percentages exceeding 50 %). Interestingly, the active hits had significantly different chemical scaffolds than the training molecules, which should enhance confidence in the dbCICA modeling strategy and the corresponding pharmacophores (i.e., the models were robust enough to allow scaffold hopping without any loss of bioactivity). Furthermore, a detailed examination of the docked poses of the active hits shows they share binding-site contacts with the training compounds; moreover, they fit the corresponding pharmacophoric models in a similar manner to the training molecules. Figures 10 and 11 show how three of the retrieved hits dock into the ATPase

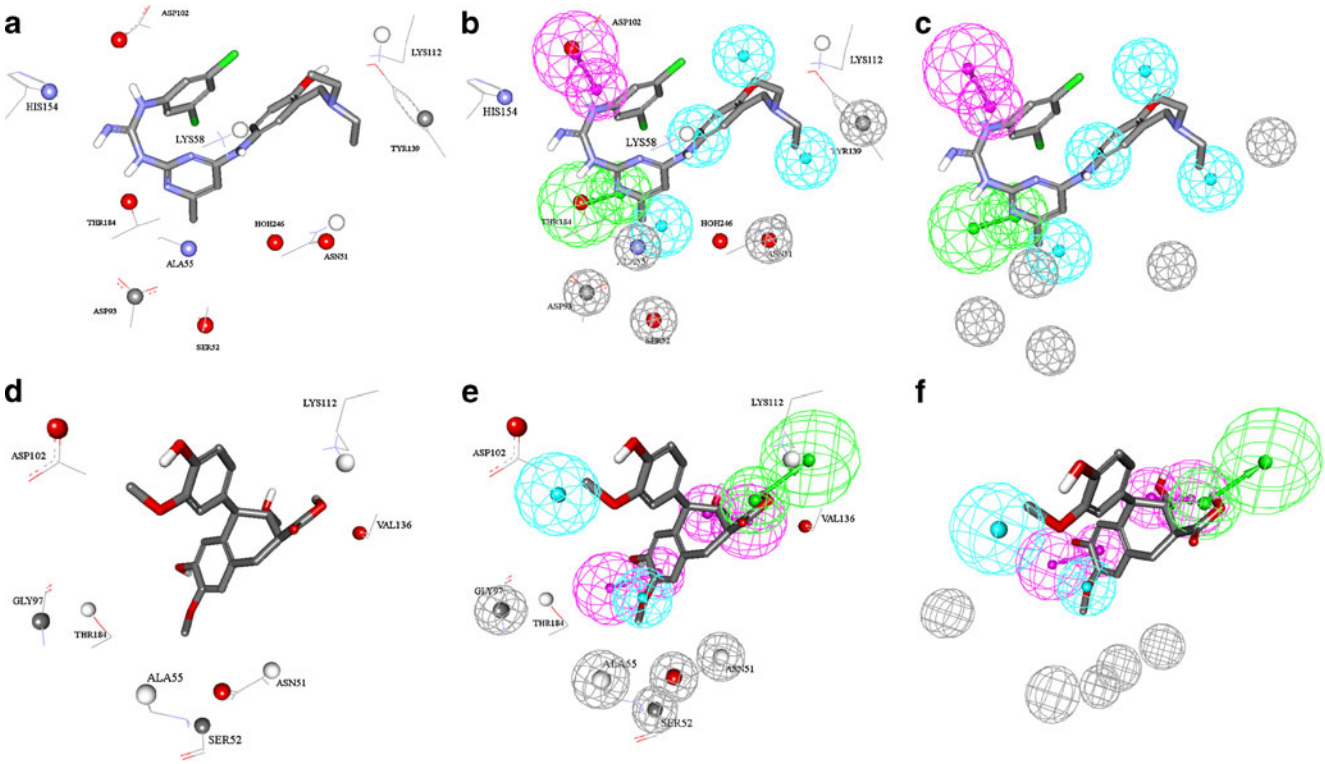

Fig. 11 **a** The docked pose of hit **92** (Fig. 9 and Table 6), employing the docking conditions of model II (Tables 1 and 2). **b** The docked pose of **92** and how it relates to the pharmacophoric features of Hypo-II. **c** Mapping the docked pose of **92** to Hypo-II. **d** The docked pose of hit **89** (Fig. 9 and Table 6), employing the docking conditions of model III (Tables 1 and 2). **e** The docked pose of **89** and how it relates to the pharmacophoric features of Hypo-III. **f** Mapping the docked pose of **89** to Hypo-III

binding pocket of Hsp90α, and how they map onto the corresponding pharmacophores.

Conclusions

In the current study, we implemented our new methodology—docking-based comparative intermolecular contacts analysis (dbCICA)—in order to find the optimal docking configurations that were required to fit 83 Hsp90α inhibitors into the ATPase-binding pocket of this chaperone. Furthermore, the optimal dbCICA models were translated into valid pharmacophoric models that were used as 3D search queries to find new Hsp90α inhibitors in the NCI structural database. Fifteen hits exhibited significant inhibitory profiles against Hsp90α (i.e., with inhibition percentages exceeding 50 %). Our novel approach proved to be useful for validating the docking conditions of Hsp90α and as means to screen virtual compound libraries for new hits.

References

1. Mahalingam D, Swords R, Carew JS, Nawrocki ST, Bhalla K, Giles FJ (2009) Targeting HSP90α for cancer therapy. Br J Cancer 100:1523–1529
2. Chiosis G, Rodina A, Moulick K (2006) Emerging Hsp90α inhibitors: from discovery to clinic. Anti Cancer Agents Med Chem 6:1–8
3. Dymock BW, Drysdale MJ, McDonald E, Workman P (2004) Inhibitors of Hsp90α and other chaperones for the treatment of cancer. Expert Opin Ther Pat 14:837–847
4. Isaacs JS, Xu W, Neckers L (2003) Heat shock protein 90 as a molecular target for cancer therapeutics. Cancer Cell 3:213–217
5. Pearl LH, Prodromou C, Workman P (2008) The Hsp90α molecular chaperone: an open and shut case for treatment. Biochem J 41:439–453
6. Neckers L, Schulte TW, Mimnaugh E (1999) Geldanamycin as a potential anti-cancer agent: its molecular target and biochemical activity. Invest New Drugs 17:361–373
7. Soga S, Shiotsu Y, Akinaga S, Sharma SV (2003) Development of radicicol analogues. Curr Cancer Drug Targets 3:359–369
8. Chiosis G, Kang Y, Sun W (2008) Discovery and development of purine scaffold Hsp90α inhibitors. Expert Opin Drug Discov 3:99–114
9. Hwangseo P, Yun-Jung K, Ji-Sook H (2007) A novel class of Hsp90α inhibitors isolated by structure-based virtual screening. Bioorg Med Chem Lett 17:6345–6349
10. Barril X, Beswick M, Collier A, Drysdale M, Dymock B, Fink A, Grant K, Howes R, Jordan A, Massey A (2006) 4-Amino derivatives of the Hsp90α inhibitor CCT018159. Bioorg Med Chem Lett 16:2543–2548
11. Barril X, Brough P, Drysdale M, Hubbard RE, Massey A, Surgenor A, Wright L (2005) Structure-based discovery of a new class of Hsp90α inhibitors. Bioorg Med Chem Lett 15:5187–5191
12. Chiosis G, Lucas B, Shtil A, Huezoa H, Rosen N (2002) Development of a purine-scaffold novel vlass of Hsp90α binders that inhibit the proliferation of cancer cells and induce the degradation of Her2tyrosine kinase. Bioorg Med Chem 10:3555–3564
13. Neckers L (2006) Using natural product inhibitors to validate Hsp90α as a molecular target in cancer. Curr Top Med Chem 6:1163–1171
14. Xiao L, Lu X, Ruden DM (2006) Effectiveness of Hsp90α inhibitors as anti-cancer drugs. Mini-Rev Med Chem 6:1137–1143
15. Neckers L, Mollapour M, Tsutsumi S (2009) The complex dance of the molecular chaperone Hsp90. Trends Biochem Sci 34:223–226
16. Jeffrey RH, Chang P, Andrew MP, Aaron RK, Michael DW, Xilu W, Christopher LL, Jamey CM, Kerry MS, Russell AJ, Jun C, Paul LR, Sha J, Stephen KT, Edward DM, Sarah AD, Uri SL, Jean MS, Karl AW, Diane MB, Stephen WF, Steven WE, Philip JH (2007) Discovery and design of novel HSP90A inhibitors using multiple fragment-based design strategies. Chem Biol Drug 70:1–12
17. Taha MO, Habash M, Al-Hadidi Z, Al-Bakri A, Younis K, Sisan S (2011) Docking-based comparative intermolecular contacts analysis as new 3-D QSAR concept for validating docking studies and in silico screening: NMT and GP inhibitors as case studies. J Chem Inf Model 51:647–669
18. Morris GM, Olson AJ, Goodsell DS (2000) Protein–ligand docking methods. Princ Med Chem 8:31–48
19. Kontoyianni M, McClellan LM, Sokol GS (2004) Evaluation of docking performance: comparative data on docking algorithms. J Med Chem 47:558–565
20. Beier C, Zacharias M (2010) Tackling the challenges posed by target flexibility in drug design. Expert Opin Drug Dis 5:347–359
21. Boyd S (2007) FlexX suite. Chem World UK 4:72
22. Rarey M, Kramer B, Lengauer T, Klebe G (1996) A fast flexible docking method using an incremental construction algorithm. J Mol Biol 261:470–489
23. Ewing TJA, Makino S, Skillman AG, Kuntz ID (2001) DOCK 4.0: search strategies for automated molecular docking of flexible molecule databases. J Comput Aid Mol Des 15:411–428
24. Jones G, Willett P, Glen RC, Leach AR, Taylor R (1997) Development and validation of a genetic algorithm for flexible docking. J Mol Biol 267:727–748
25. Vaque M, Ardrevol A, Blade C, Salvado MJ, Blay M, Fernandez-Larrea J, Arola L, Pujadas G (2008) Protein–ligand docking: a review of recent advances and future perspectives. Curr Pharm Anal 4:1–19
26. Cosconati S, Forli S, Perryman AL, Harris R, Goodsell DS, Olson AJ (2010) Virtual screening with AutoDock: theory and practice. Expert Opin Drug Dis 5:597–607
27. Morris GM, Goodsell DS, Halliday RS, Huey R, Hart WE, Belew RK, Olson AJ (1998) Automated docking using a Lamarckian genetic algorithm and an empirical binding free energy function. J Comput Chem 19:1639–1662
28. Halgren TA, Murphy RB, Friesner RA, Beard HS, Frye LL, Pollard WT, Banks JL (2004) Glide: a new approach for rapid, accurate docking and scoring. 2. Enrichment factors in database screening. J Med Chem 47:1750–1759
29. Accelrys Inc. (2000) Cerius2 LigandFit 4.10. Accelrys Inc., San Diego
30. Diller DJ, Merz KM (2001) High throughput docking for library design and library prioritization. Proteins 43:113–124
31. Hecht D, Fogel GB (2009) Computational intelligence methods for docking scores. Curr Comput Aid Drug 5:56–68
32. Bissantz C, Folkers G, Rognan D (2000) Protein-based virtual screening of chemical databases. 1. Evaluation of different docking/scoring combinations. J Med Chem 43:4759–4767
33. Gao WR, Lai YL (1998) SCORE: a new empirical method for estimating the binding affinity of a protein–ligand complex. J Mol Model 4:379–394
34. Krammer A, Kirchhoff PD, Jiang X, Venkatachalam CM, Waldman M (2005) LigScore: a novel scoring function for predicting binding affinities. J Mol Graph Model 23:395–407
35. Velec HFG, Gohlke H, Klebe G (2005) Drug score-knowledge-based scoring function derived from small molecule crystal data

with superior recognition rate of near-native ligand poses and better affinity prediction. J Med Chem 48:6296–6303
36. Jain AN (2006) Scoring functions for protein–ligand docking. Curr Protein Pept Sci 7:407–420
37. Rajamani R, Good AC (2007) Ranking poses in structure-based lead discovery and optimization: current trends in scoring function development. Curr Opin Drug Disc 10:308–315
38. Krovat EM, Langer T (2004) Impact of scoring functions on enrichment in docking- based virtual screening: an application study on renin inhibitors. J Chem Inf Comput Sci 44:1123–1129
39. Foloppe N, Hubbard R (2006) Towards predictive ligand design with free-energy based computational methods? Curr Med Chem 13:3583–3608
40. Englebienne P, Moitessier N (2009) Docking ligands into flexible and solvated macromolecules. Are popular scoring functions accurate for this class of proteins? J Chem Inf Model 49:1568–1580
41. Jain AN (1996) Scoring non-covalent protein–ligand interactions: a continuous differentiable function tuned to compute binding affinities. J Comput Aided Mol Des 10:427–440
42. Böhm HJ (1998) Prediction of binding constants of protein ligands: a fast method for the prioritization of hits obtained from de novo design or 3D database search programs. J Comput Aided Mol Des 12:309–323
43. Eldridge MD, Murray CW, Auton TR, Paolini GV, Mee RP (1997) Empirical scoring functions: I. The development of a fast empirical scoring function to estimate the binding affinity of ligands in receptor complexes. J Comput Aided Mol Des 11:425–445
44. Wang R, Gao Y, Lai L (1998) SCORE: a new empirical method for estimating the binding affinity of a protein–ligand complex. J Mol Model 4:379–394
45. Gehlhaar DK, Bouzida D, Rejto P (1999) Reduced dimensionality in ligand–protein structure prediction: covalent inhibitors of serine proteases and design of site-directed combinatorial libraries. In: Parrill L, Rami Reddy M (eds) Rational drug design: novel methodology and practical applications. American Chemical Society, Washington, DC, pp 292–311
46. Wang R, Lai L, Wang S (2002) Further development and of empirical scoring functions for structure-based binding validation affinity prediction. J Comput Aided Mol Des 16:11–26
47. Muegge I, Martin YC (1999) A general and fast scoring function for protein–ligand interactions: a simplified potential approach. J Med Chem 42:791–804
48. Muegge I (2000) A knowledge-based scoring function for protein–ligand interactions: probing the reference state. Perspect Drug Discov 20:99–114
49. Muegge I (2001) Effect of ligand volume correction on PMF scoring. J Comput Chem 22:418–425
50. Gohlke H, Hendlich M, Klebe G (2000) Knowledge-based scoring function to predict protein–ligand interactions. J Mol Biol 295:337–356
51. Muegge I (2006) PMF scoring revisited. J Med Chem 49:5895–5902
52. Song CM, Lim SJ, Tong JC (2009) Recent advances in computer-aided drug design. Brief Bioinform 10:579–591
53. Jorgensen WL (2009) Efficient drug lead discovery and optimization. Acc Chem Res 42:724–733
54. Leach AR, Shoichet BK, Peishoff CE (2006) Prediction of protein–ligand interactions. Docking and scoring: successes and gaps. J Med Chem 49:5851–5855
55. Klebe G (2006) Virtual ligand screening: strategies, perspectives and limitations. Drug Discov Today 11:580–594
56. Krissinel E (2009) Crystal contacts as nature's docking solutions. J Comput Chem 31:133–143
57. Steinbrecher T, Labahn A (2010) Towards accurate free energy calculations in ligand protein-binding studies. Curr Med Chem 17:767–785
58. Taha MO, AlDhamin M (2005) Effects of variable docking conditions and scoring functions on the qualities of protein aligned CoMFA models constructed from diverse h-PTP 1B inhibitors. J Med Chem 48:8016–8034
59. Tame JRH (1999) Scoring functions: a view from the bench. J Comput Aided Mol Des 13:99–108
60. Kollman P (1993) Free energy calculations: applications to chemical and biochemical phenomena. Chem Rev 93:2395–2417
61. Homans SW (2007) Water, water everywhere—except where it matters. Drug Discov Today 12:534–539
62. Poornima CS, Dean PM (1995) Hydration in drug design. 1. Multiple hydrogen-bonding features of water molecules in mediating protein–ligand interactions. J Comput Aided Mol Des 9:500–512
63. Poornima CS, Dean PM (1995) Hydration in drug design. 2. Influence of local site surface shape on water binding. J Comput Aided Mol Des 9:513–520
64. Poornima CS, Dean PM (1995) Hydration in drug design. 3. Conserved water molecules at the ligand-binding sites of homologous proteins. J Comput Aided Mol Des 9:521–531
65. Koehler KF, Rao SN, Snyder JP (1996) Modeling drug–receptor interactions. In: Cohen NC (ed) Guidebook on molecular modeling in drug design. Academic, San Diego, pp 235–336
66. Pastor M, Cruciani G, Watson K (1997) A strategy for the incorporation of water molecules present in a ligand binding site into a three-dimensional quantitative structure–activity relationship analysis. J Med Chem 40:4089–4102
67. Silverman RA (1991) The organic chemistry of drug design and drug action. Academic, San Diego, pp 62–65
68. Waszkowycz B (1998) New methods for structure-based de novo drug design. In: Harvey AL (ed) Advances in drug discovery techniques. Wiley, Chichester, pp 150–153
69. Sutherland JJ, Nandigam RK, Erickson JA, Vieth M (2007) Lessons in molecular recognition. 2. Assessing and improving cross-docking accuracy. J Chem Inf Model 47:2293–2302
70. Verdonk ML, Berdini V, Hartshorn MJ, Mooij WTM, Murray CW, Watson P (2004) Virtual screening using protein–ligand docking: avoiding artificial enrichment. J Chem Inf Comput Sci 44:793–806
71. Wang R, Lu Y, Wang S (2003) Comparative evaluation of 11 scoring functions for molecular docking. J Med Chem 46:2287–2303
72. Abu-Hammad AM, Afifi F, Taha MO (2007) Combining docking, scoring and molecular field analyses to probe influenza neuraminidase–ligand interactions. J Mol Graph Model 26:443–456
73. Abu-Hammad A, Zalloum WA, Zalloum H, Abu-Sheikha G, Taha MO (2009) Homology modeling of MCH1 receptor and validation by docking/scoring and protein-aligned CoMFA. Eur J Med Chem 44:2583–2596
74. Venkatachalam CM, Jiang X, Oldfield T, Waldman M (2003) LigandFit: a novel method for the shape-directed rapid docking of ligands to protein active sites. J Mol Graph Model 21:289–307
75. Brough PA, Aherne W, Barril X, Borgognoni J, Boxall K, Cansfield JE, Cheung K-MJ et al (2008) 4,5-Diarylisoxazole Hsp90α chaperone inhibitors: potential therapeutic agents for the treatment of cancer. J Med Chem 51:196–218
76. McDonald E, Jones K, Brough PA, Drysdale MJ, Workman P (2006) Discovery and development of pyrazole-scaffold Hsp90α inhibitors. Curr Top Med Chem 6:1193–1203
77. Gopalsamy A, Shi M, Golas J, Vogan E, Jacob J, Johnson M, Lee F, Nilakantan R, Petersen R, Svenson K, Chopra R, Tam MS, Wen Y, Ellingboe J, Arndt K, Boschelli F (2008) Discovery of benzisoxazoles as potent inhibitors of chaperone heat shock protein 90. J Med Chem 51:373–375
78. Gasteiger J, Marsili M (1980) Iterative partial equalization of orbital electronegativity—a rapid access to atomic charges. Tetrahedron 36:3219–3228
79. Gehlhaar DK, Verkhivker GM, Rejto PA, Sherman CJ, Fogel DB, Fogel LJ, Freer ST (1995) Molecular recognition of the inhibitor

AG-1343 by HIV-1 protease: conformationally flexible docking by evolutionary programming. Chem Biol 2:317–324
80. Accelrys Inc. (2009) Discovery Studio 2.5. Accelrys Inc., San Diego
81. Taha MO, Al-Bakri AG, Zalloum WA (2006) Discovery of potent inhibitors of pseudomonal quorum sensing via pharmacophore modeling and in silico screening. Bioorg Med Chem Lett 16:5902–5906
82. Taha MO, Bustanji Y, Al-Bakri AG, Al-Motassem Y, Zalloum WA, Al-Masri IM, Atallah N (2007) Discovery of new potent human protein tyrosine phosphatase inhibitors via pharmacophore and QSAR analysis followed by in silico screening. J Mol Graph Model 25:870–884
83. Avila C, Hadden MK, Ma Z, Kornilayev BA, Ye QZ, Blagg BS (2006) Highthroughput screening for Hsp90α ATPase inhibitors. Bioorg Med Chem Lett 16:3005–3008
84. Lanzetta PA, Alvarez LJ, Reinach PS, Candia OA (1979) An improved assay for nanomole amounts of inorganic phosphate. Anal Biochem 100:95–97
85. Christopher A, Boris AK, Brian SJ (2006) Development and optimization of a useful assay for determining Hsp90s inherent ATPase activity. Bioorg Med Chem 14:1134–1142
86. Abu Sheikha G, Al-Sha'er MA, Taha MO (2011) Some sulfonamide drugs inhibit ATPase activity of heat shock protein 90: investigation by docking simulation and experimental validation. J Enzym Inhibit Med Chem 26:603–609
87. Al-Sha'er MA, Taha MO (2010) Elaborate ligand-based modeling reveal new nanomolar heat shock protein 90a inhibitors. J Chem Inf Model 50:1706–1723
88. Al-masri IM, Mohammad MK, Taha MO (2008) Discovery of DPP IV inhibitors by pharmacophore modeling and QSAR analysis followed by in silico screening. Chem Med Chem 3:1763–1779
89. Al-Sha'er MA, Taha MO (2010) Discovery of novel CDK1 inhibitors by combining pharmacophore modeling, QSAR analysis and in silico screening followed by in vitro bioassay. Eur J Med Chem 45:4316–4330
90. Irwin JJ, Shoichet BK (2005) ZINC—a free database of commercially available compounds for virtual screening. J Chem Inf Model 45:177–182
91. Kirchmair J, Markt P, Distinto S, Wolber G, Langer T (2008) Evaluation of the performance of 3D virtual screening protocols: RMSD comparisons, enrichment assessments, and decoy selection. What can we learn from earlier mistakes? J Comput Aided Mol Des 22:213–228
92. Jacobsson M, Liden P, Stjernschantz E, Bostroem H, Norinder U (2003) Improving structure-based virtual screening by multivariate analysis of scoring data. J Med Chem 46:5781–5789
93. Triballeau N, Acher F, Brabet I, Pin JP, Bertrand HO (2005) Virtual screening workflow development guided by the "receiver operating characteristic" curve approach. Application to high-throughput docking on metabotropic glutamate receptor subtype. J Med Chem 48:2534–2547
94. Lipinski CA (2004) Lead- and drug-like compounds: the rule-of-five revolution. Drug Discov Today Technol 1:337–341
95. Howes R, Barril X, Dymock BW, Grant K, NorthWeld CJ, Robertson AGS, Surgenor A, Wayne J, Wright L, James K, Matthews T, Cheung KM, McDonald E, Workman P, Drysdale MJ (2006) A fluorescence polarization assay for inhibitors of Hsp90. Anal Biochem 350:202–213